Electronic Supplementary Material (ESI) for Journal of Materials Chemistry B.

Precise fibrin decomposition and tumor mechanics modulation with hydroxyethyl starch-based smart nanomedicine for enhanced antitumor efficacy

Jitang Chen[a], Zhijie Zhang[a], Yining Li[a], Haowen Zeng[a], Zheng Li[a], Chong Wang[a], Chen Xu[a], Qingyuan Deng[a], Qiang Wang[a], Xiangliang Yang[a,b,c,d,e], Zifu Li[a,b,c,d,f,*]

[a] National Engineering Research Center for Nanomedicine, College of Life Science and Technology, Huazhong University of Science and Technology, Wuhan, 430074, P. R. China

[b] Key Laboratory of Molecular Biophysics of Ministry of Education, College of Life Science and Technology, Huazhong University of Science and Technology, Wuhan, 430074, P. R. China

[c] Hubei Key Laboratory of Bioinorganic Chemistry and Materia Medical, Huazhong University of Science and Technology, Wuhan, 430074, P. R. China

[d] Hubei Engineering Research Center for Biomaterials and Medical Protective Materials, Huazhong University of Science and Technology, Wuhan, 430074, P. R. China

[e] GBA Research Innovation Institute for Nanotechnology, Guangdong, 510530, P. R. China

[f] Wuhan Institute of Biotechnology, High Tech Road 666, East Lake high tech Zone, Wuhan, 430040, P. R. China

* Correspondence and requests for materials should be addressed to ZFL (email: zifuli@hust.edu.cn).

Abstract

Chemotherapy is a conventional cancer treatment in clinical settings. Although numerous nano drug delivery systems have been developed, the chemotherapeutic effect is greatly limited by abnormal tumor mechanics in solid tumors. Tumor stiffening and accumulated solid stress compress blood vessels and inhibit drug delivery to tumor cells, becoming critical challenges for chemotherapy. By loading doxorubicin (DOX), tissue plasminogen activator (tPA), and fibrin targeting peptide CREKA (Cys-Arg-Glu-Lys-Ala) within pH responsive amphiphilic block polymers, pyridyldithio-hydroxyethyl starch-Schiff base-polylactic acid (PA-HES-pH-PLA), we report a smart nanomedicine, DOX@CREKA/tPA-HES-pH-PLA (DOX@CREKA/tPA-HP), which exhibits a potent antitumor efficacy. In triple-negative breast cancer (TNBC) 4T1 tumors, DOX@CREKA/tPA-HP precisely targeted and effectively decomposed fibrin matrix. By measuring Young's Modulus of tumor slices and quantifying tumor openings, we demonstrated that DOX@CREKA/tPA-HP remarkably reduced tumor stiffness and solid stress. Consequently, the alleviated tumor mechanics decompressed tumor blood vessels, promoted drug delivery, and led to amplified antitumor effect. Our work reveals that decomposing fibrin is a significant means for modulating tumor mechanics, and DOX@CREKA/tPA-HP is a promising smart nanomedicine for treating TNBC.

Keywords:

tissue plasminogen activator (tPA), fibrin decomposition, tumor mechanics, hydroxyethyl starch (HES), chemotherapy, smart nanomedicine

Introduction

Chemotherapy is a conventional treatment for a variety of cancers. However, the clinical efficacy of chemotherapy is unsatisfactory. For solid tumors, abnormal tumor mechanics regulate cancer cells and restrict drug delivery, becoming critical challenges for successful cancer treatment. One of the pivotal features of abnormal tumor mechanics is the extremely higher stiffness of tumor tissues than that of healthy tissues.[1-5] High rigidity is due to the fibrosis of malignant tissues, which is often used as a diagnostic marker and a prognostic factor in clinical practice.[5, 6] Another key trait is the cumulative solid stress mainly caused by rapid proliferation of cancer cells and accumulation of extracellular matrix (ECM).[7, 8] Both characteristics can activate a cascade of mechanical feed-back loops that promote tumorigenesis, progression,[9, 10] invasion, metastasis,[11-14] and induce drug resistance.[15] Simultaneously, solid stress compresses blood vessels and reduces tumor blood perfusion, thereby hindering drug delivery to tumors and impeding intratumoral drug distribution.[16] Therefore, it is urgent to develop effective means to modulate abnormal tumor mechanics for enhanced chemotherapeutic effect.

Recently, tremendous efforts have been devoted to modulating tumor mechanics. Disrupting tumor hypoxia by hyperbaric oxygen (HBO) therapy can constrain cancer-associated fibroblasts (CAFs) in pancreatic ductal adenocarcinoma (PDAC).[17] As CAFs are the main producers of ECM, HBO can efficiently reduce collagen I and fibronectin in PDAC Panc02 tumors,[17] triple negative breast cancer (TNBC) 4T1 tumors,[18] and hepatocellular carcinoma (HCC) H22 tumors,[19] leading to reduced stiffness, alleviated solid stress, and normalized blood vessels. In PDAC models, down-regulating collagen I and hyaluronic acid (HA) by losartan also alleviates solid stress and decompresses blood vessels, thus enhancing chemotherapeutic effect and increasing overall survival.[20] In human breast MCF-7 tumor-bearing mice models, eliminating collagen by collagenase and paclitaxel (PTX) prodrug co-loaded nanozyme (SP-NE) can significantly remodel ECM mechanics and enhance chemosensitivity.[21] These studies corroborate that degrading matrix components such as collagen, HA, and fibronectin can regulate abnormal tumor mechanics, promote drug delivery efficiency, and

augment antitumor efficacy.

Fibrin is another important extracellular matrix component that has gained increasing concerns.[22-25] Fibrin matrix is formed by cross-linking of fibrinogen that leaks from abnormal tumor blood vessels.[26, 27] The ratio of the fibrin area in different tumors ranges from 20% to 90%.[23] Fibrin promotes tumor progression through the following mechanisms. First, fibrin forms a physical barrier that protects cancer cells from being recognized and eradicated by the immune system.[28] Second, fibrin helps circulating tumor cells resist the scavenging effect of natural killer cells and enhances metastatic potential of tumor cells.[29] Third, fibrin plays a vital role in promoting tumor angiogenesis.[30] Last but not the least, fibrin impedes drug delivery to tumor cells and diminishes antitumor effect of conventional chemotherapeutic drugs.[22] Several researches have reported that eliminating fibrin by tissue plasminogen activator (tPA) can promote drug delivery to cancer cells. For instance, administration of free tPA increases the diameter of tumor blood vessels and promotes intratumoral distribution of Doxil and PTX-loaded nanoparticles in B16F10 tumors[23] and A549 tumors,[22] respectively. In C-26 colon cancer models, tPA-installed redox-active nanoparticle (tPA@iRNP) degrades fibrin deposited in tumor tissues, contributing to enhanced penetration of iRNP and M1 macrophage via the restored blood flow.[24] However, these studies decompose intratumoral fibrin by using free tPA or simple tPA-loaded nanomedicine that lacks tumor specificity. While tPA is used as the first line therapy for acute stroke in clinical settings, the risk of tPA-induced bleeding cannot be ignored and could be fatal.[31] Therefore, it is essential to build an integrated nanoparticle that can not only precisely modulate tumor mechanics for enhanced drug delivery efficiency and augmented antitumor efficacy but also ensure safety for cancer patients in clinical practice. Notwithstanding the above explorations, the role of fibrin in tumor mechanics is elusive, calling for further study to establish the direct relationship between fibrin and abnormal tumor mechanics.

Hydroxyethyl starch (HES) is a safe biopolymer that has been used as a clinical plasma substitute for more than 50 years.[32] Modified HES has been leveraged to encapsulate drugs for prolonged plasma half-life and promoted tumor accumulation.[33-36] Based on

HES and polylactic acid (PLA), here we synthesized a pH responsive amphiphilic block polymer, pyridyldithio-hydroxyethyl starch-Schiff base-polylactic acid (PA-HES-pH-PLA). Doxorubicin (DOX) was encapsulated into the polymers by emulsion-solvent evaporation method to prepare DOX@HES-pH-PLA (DOX@HP). tPA and fibrin targeting peptide, CREKA (Cys-Arg-Glu-Lys-Ala) were then decorated on the surface of nanoparticle to form DOX@CREKA/tPA-HP (Fig. 1A). The functions of the rational designed DOX@CREKA/tPA-HP are described below. CREKA modified on the outer layer of DOX@CREKA/tPA-HP transports the nanomedicine to intratumoral fibrin area owing to its fibrin targeting capacity.[37, 38] When DOX@CREKA/tPA-HP arrives at tumor tissues, the pH responsive Schiff-base bond is cleaved at pH 6.5, tumor extracellular condition. Then HES is separated from PLA, and DOX and tPA are released. HES and PLA remaining at tumor sites will gradually degrade over time. Simultaneously, tPA contributes to the decomposition of fibrin by converting plasminogen to plasmin, which modulates tumor mechanics and promotes intratumoral blood perfusion, ultimately leading to enhanced DOX delivery and potent treatment outcomes (Fig. 1B).

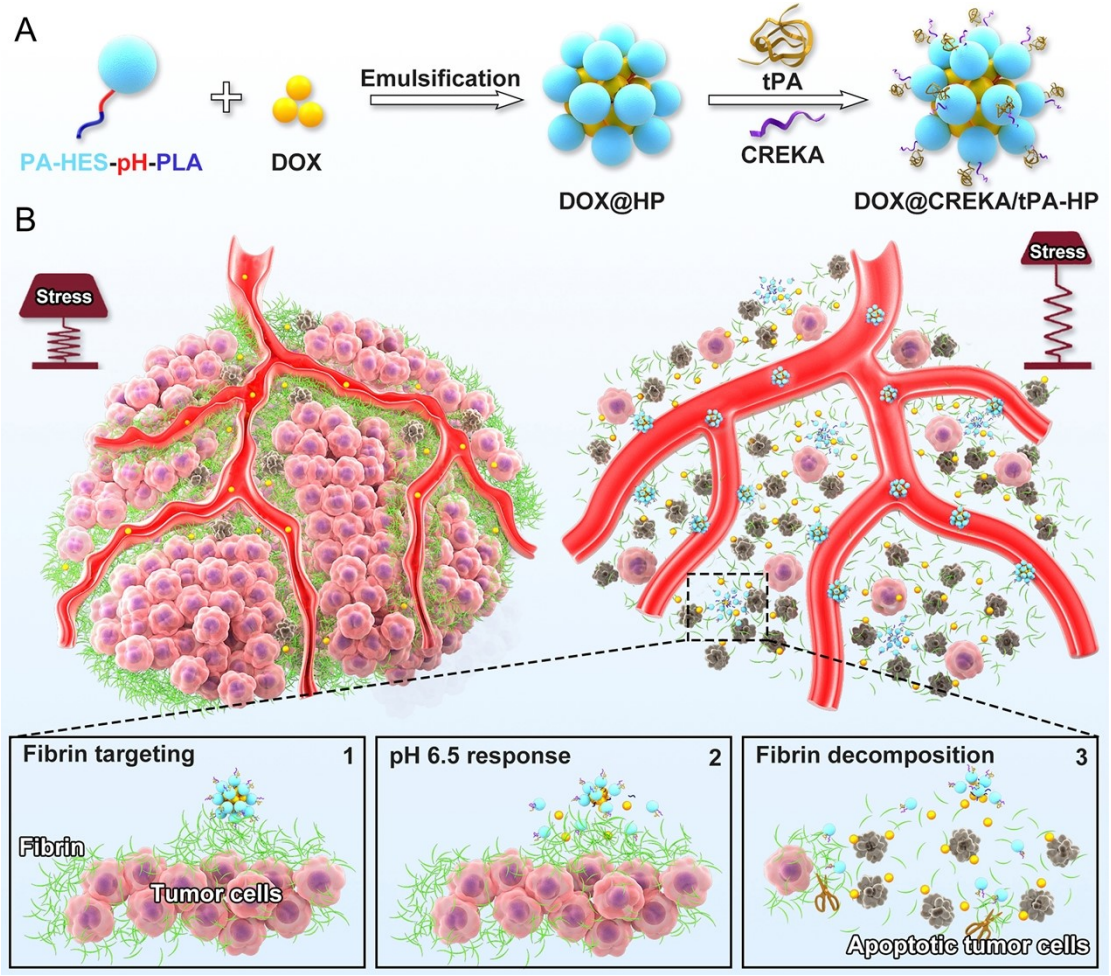

Fig. 1 Schematic illustration of precisely modulating tumor mechanics with DOX@CREKA/tPA-HP for potent antitumor efficacy. (A) Preparation of DOX@CREKA/tPA-HP. (B) DOX@CREKA/tPA-HP targets abundant fibrin in tumors by CREKA and releases DOX in weakly acidic tumor microenvironment. DOX@CREKA/tPA-HP alleviates solid stress and decompresses blood vessels by decomposing fibrin, thereby facilitating drug delivery and augmenting antitumor effect.

Materials and methods

Materials

HES with an average molecular weight (M_w) of 130 kDa and molar substitution of hydroxyethyl of 0.4 was a gift from Wuhan HUST Life Science & Technology Co., Ltd (Wuhan, China). DOX was bought from Meilunbio Inc. (Dalian, China). CREKA (purity > 95%) was synthesized by Hefei National Peptide Biotechnology Co. Ltd. (Anhui, China). tPA was purchased from Boehringer Ingelheim Pharma GmbH & Co.

KG. PLA (purity > 95%) with an average M_w of 6 kDa was bought from Jinan Daigang Biomaterials Co., Ltd. (Jinan, China). Fibrinogen, thrombin, plasminogen and D-Ile-Pro-Arg p-nitroanilide dihydrochloride (S-2288) were bought from Sigma-Aldrich. Methyl thiazolyl tetrazolium (MTT) was bought from Solarbio LifeScience Inc. (Beijing, China). RPMI 1640 cell culture medium, DMEM cell culture medium, fetal bovine serum (FBS), trypsin, penicillin-streptomycin solution, PBS and Transwell plate (6 mm diameter, 3 μm pore size, polycarbonate membrane) were purchased from Thermo Fisher Scientific. All other chemical reagents were bought from Aladdin Reagent Inc. (Shanghai, China) or China National Pharmaceutical Group Corporation.

Animals

BALB/c mice were purchased from Beijing Vital River Laboratory Animal Technology Co. Ltd. These animals were housed in a specific pathogen free environment. All animal procedures were performed in accordance with the internationally accepted principles and Guidelines for the Care and Use of Laboratory Animals of Huazhong University of Science and Technology and the experiment protocols were approved by the Institutional Animal Ethical Committee of Huazhong University of Science and Technology.

Synthesis of PA-HES-pH-PLA

Synthesis of hydroxylated HES (HES-COOH) HES (1.0 g) and NaOH (0.8 g) were dissolved in 20 mL of ultrapure water. Chloroacetic acid (1 g) was added to the above solution under stirring. The reaction was performed under 70℃ for 3 h. After that, the product was obtained by adding 200 mL of methanol and centrifuged at 5000 rpm for 10 min. The precipitate was dissolved by 20 mL of ultrapure water and dialyzed against ultrapure water for 3 days (molecular weight cut off (MWCO): 3500 Da). Finally, HES-COOH was harvested by lyophilization.

Synthesis of pyridyldithio-HES (HES-PA) HES-COOH (1.0 g), 2-(pyridyldithio)-ethylamine hydrochloride (PA·HCl, 110.2 mg), 1-(3-dimethylaminopropyl)-3-ethylcarbodiimide hydrochloride (EDCI, 191.7 mg) and N-hydroxy succinimide (NHS, 57.5 mg) were dissolved in 30 mL of ultrapure water. The mixture was stirred under argon protection at room temperature for 24 h. Then, the solution was dialyzed against

ultrapure water for 3 days (MWCO: 3500 Da) and HES-PA was obtained by lyophilization.

Synthesis of pyridyldithio-HES-aldehyde (PA-HES-ALD) HES-PA (1.0 g), 4-carboxy-benzaldehyde (83.3 mg), EDCI (228.7 mg) and 4-dimethylaminopyridine (DMAP, 67.8 mg) were dissolved in 25 mL of dimethyl sulfoxide (DMSO). The above solution was stirred under argon protection at 30℃ for 24 h. Then, the product was purified by dialyzing against ultrapure water for 3 days (MWCO: 3500 Da) and PA-HES-ALD was harvested by lyophilization.

Synthesis of amino-terminated PLA (PLA-NH_2) PLA (90.0 mg), 1,6-hexanediamine (17.4 mg), EDCI (57.5 mg) and NHS (34.5 mg) were dissolved in 10 mL of DMSO. The solution was stirred at 40℃ for 48 h to obtain PLA-NH_2. The product was precipitated by dialyzing against ultrapure water for 3 days (MWCO: 1000 Da). After that, PLA-NH_2 was acquired by lyophilization.

Synthesis of PA-HES-pH-PLA PA-HES-pH-PLA was synthesized by Schiff base reaction. PA-HES-ALD (0.5 g) and PLA-NH_2 (46.2 mg) was dissolved in 15 mL of DMSO. Then, a drop of acetic acid was added to the mixture. The solution was stirred under argon protection at 30℃ for 24 h. The product was precipitated by mixed solvent (petroleum ether: isopropanol = 1: 1, V/V) and washed for 3 times. Finally, PA-HES-pH-PLA was obtained by vacuum drying.

Characterization of PA-HES-pH-PLA

HES-PA, PA-HES-ALD and PA-HES-pH-PLA were characterized by proton nuclear magnetic resonance (^{1}H NMR) spectra. The degree of PLA substitution for PA-HES-pH-PLA (DS_{PLA}) was calculated by analyzing data of PA-HES-pH-PLA from ^{1}H NMR spectra. The peaks at the range between 4.4 and 5.7 ppm of PA-HES-pH-PLA belong to the protons of anhydroglucose units (AGU) in HES and the protons of methine groups in PLA chains. The peaks at 1.47 ppm of PA-HES-pH-PLA belong to the protons of methyl groups in PLA chains.

The relative number of PLA molecules and HES molecules were calculated using the following formula:

$$\text{relative number of PLA molecules} = \frac{ICH3}{3} \times \frac{1}{nPLA}$$

$$\text{relative number of HES molecules} = \frac{IAGU + CH - \frac{ICH3}{3}}{4} \times \frac{1}{nHES}$$

I_{CH3} is the integral area of the proton peaks of methyl groups in PLA that locate at 1.47 ppm. $I_{AGU + CH}$ is the integral area of the proton peaks of methine groups in PLA and AGU in HES that locate at the range between 4.4 and 5.7 ppm. n_{PLA} represents the degree of polymerization of PLA, and n_{HES} represents the numbers of AGU of one HES molecule.

DS_{PLA} was calculated using the following formula:

$$DSPLA = \frac{\text{relative number of PLA molecules}}{\text{relative number of HES molecules}}$$

Cytotoxicity of PA-HES-pH-PLA

4T1 cells and 3T3 fibroblasts were used to evaluate the biological safety of PA-HES-pH-PLA. Briefly, 4T1 cells or 3T3 fibroblasts were seeded in 96-well plates at a density of 5×10^3 cells and incubated overnight. Then, the cells were incubated with PA-HES-pH-PLA solutions with various concentrations (0, 40, 100, 200 and 400 μg/mL) for about 24 h. The safety of PA-HES-pH-PLA were evaluated by the cell viabilities tested by CCK8 assay.

Preparation of DOX@CREKA/tPA-HP

DOX@CREKA/tPA-HP was prepared by the emulsion-solvent evaporation method (Fig. 1A). First, DOX was prepared by reacting 1 mg of DOX·HCl with 0.8 μL of triethylamine in 150 μL of mixed organic solvent (dichloromethane: methyl alcohol = 2: 1, V/V) for 30 min. PA-HES-pH-PLA (10 mg) was dissolved in 2 mL of PBS buffer (pH 7.4). Then, the hydrophobic DOX in 150 μL of mixed solvent was added to water phase. The mixture was then sonicated for 3 min at 150 W (Scientz-IID, Ningbo Scientz Biotechnology Co., Ltd). Afterward, the organic solvent was removed by vacuum evaporation and DOX@HP was obtained. Then, tPA and CREKA were added to the obtained product and mixed overnight for decorating on the surface of the nanoparticle

through disulfide exchange between sulfhydryl group of cysteine and pyridyl disulfide moiety on nanoparticle.[39, 40] At last, DOX@CREKA/tPA-HP was purified by ultrafiltration device (MWCO: 100,000 Da, Millipore).

Calculation of drug loading content

The amount of DOX loaded in nanoparticles was detected by testing the absorbance of DOX at 492 nm. The weight of tPA in nanoparticles was tested by Bradford Protein Assay Kit (Beyotime Biotechnology, P0006C). The weight of CREKA loaded in nanoparticles was detected by indirect approach. Briefly, the underlying filtrate from ultrafiltration device was collected after purification of DOX@CREKA/tPA-HP. The amount of CREKA in the filtrate was tested by high performance liquid chromatography (HPLC). Then, the amount of CREKA loaded in nanoparticles was calculated by the total amount of CREKA minus the amount of CREKA in the filtrate. Drug loading content (DLC) and drug loading efficiency (DLE) were calculated using the following formulas:

$$\text{DLC} = \frac{\text{weight of drug in } the \text{ nanoparticles}}{\text{weight of } the \text{ nanoparticles}} \times 100\%$$

$$\text{DLE} = \frac{\text{weight of drug in } the \text{ nanoparticles}}{\text{weight of } the\ added\ drug} \times 100\%$$

Characterization of DOX@CREKA/tPA-HP

The diameter and morphology of DOX@CREKA/tPA-HP were characterized by dynamic light scattering (DLS, Malvern Zetasizer Nano-ZS, U.K.), transmission electron microscopy (TEM, JEM-1230; JEOL, Japan), and atomic force microscopy (AFM, Multimode 8; Bruker). The stability of DOX@CREKA/tPA-HP in PBS was detected for 7 days by DLS and the stability of DOX@CREKA/tPA-HP in 10% FBS solution was detected for 48 h by DLS as well. Cumulative release of DOX was measured by dialysis bag (MWCO: 3500 Da). DOX@CREKA/tPA-HP was added in a dialysis bag before being immersed in 30 mL of buffer solution containing 0.5% Tween 80 with different pH values. The device was placed in a shaker and shaken at 180 rpm in the condition of 37℃. 200 μL of solution was taken out at predetermined time points (0, 0.5, 1, 2, 4, 6, 8, 12, 24 and 48 h) for measurement. Then, 200 μL of fresh buffer

was added to the solution. The released DOX content was detected and calculated by the fluorescence intensity of DOX using a multimode microplate reader (Molecular Devices, Flex Station 3).

Measurement of tPA activity

The fibrinolytic activity of tPA on the surface of nanoparticle was tested by a chromogenic substrate, S-2288.[41] Briefly, the sample was added to 1.0 mM S-2288 solution (buffer: Tris-HCl, pH 7.4) and incubated at 37°C. The enzymatic activity was calculated by △Abs per min at 405 nm for 0.5 h of reaction.

Evaluation of fibrin targeting effect of DOX@CREKA/tPA-HP

Fibrin gel was constructed in a 96-well black plate. Briefly, fibrinogen (2 mg mL^{-1}) was dissolved in PBS at ice bath. Thrombin was added to the fibrinogen solution to make sure the concentration was 1 U mL^{-1}. 100 μL of fibrinogen solution was then quickly introduced into bottom of plate. The 96-well black plate was incubated at 37°C overnight to allow fibrin gel formation. Then, 200 μL of DOX@tPA-HP and DOX@CREKA/tPA-HP (10 μg mL^{-1} as DOX) were placed on the top of fibrin gels. After 1 h of incubation, the nanoparticle suspensions were removed, and the fibrin gels were washed by PBS for 3 times. The fluorescence intensities were detected by *in vivo* imaging system (IVIS Lumina XR, Caliper, U.S.). The fibrin targeting ability of CREKA was characterized by the content of the residual nanoparticles on fibrin gels.

Migration across fibrin gel

We used Transwell assay to determine the migration of DOX@CREKA/tPA-HP across fibrin gel. The fibrin gel was prepared *in situ* in the top insert of a Transwell plate (6 mm diameter, 3 μm pore size, polycarbonate membrane). Fibrinogen (2 mg mL^{-1}) was dissolved in PBS at ice bath. Then, thrombin and plasminogen were added to the fibrinogen solution to make sure the concentrations were 1 U mL^{-1} and 0.1 U mL^{-1}, respectively. 750 μL of fibrinogen solution was then quickly introduced into the top inserts. The Transwell plate was incubated at 37°C overnight to allow fibrin gel formation.

To determine the migration of DOX@CREKA/tPA-HP across fibrin gel, 1 mL of PBS was added in the bottom well of the Transwell plate. Then, six groups of 100 μL of

samples, DOX solution, DOX + tPA solution, DOX@HP suspension, DOX@HP + tPA suspension, DOX@tPA-HP suspension and DOX@CREKA/tPA-HP suspension (the content of DOX and tPA was 20 μg and 25 μg, respectively) were placed on the top of the fibrin gels. At predetermined time points (0, 1, 2, 3, 4, 6, 8 and10 h), 100 μL of PBS buffer in bottom well was taken out for following measurement, and 100 μL of fresh PBS was added back to bottom well. The cumulative amount of DOX across fibrin gel was determined and calculated by the fluorescence intensity of DOX using a multimode microplate reader.

Cellular uptake of DOX@CREKA/tPA-HP across fibrin gel

Cellular uptake of DOX@CREKA/tPA-HP across fibrin gel was determined by Transwell assay as well. Fibrin gel was prepared as described above. 1×10^6 4T1 cells were seeded in the bottom well. After 4T1 cells were cultured for 24 h, six groups of 100 μL of samples, DOX solution, DOX + tPA solution, DOX@HP suspension, DOX@HP + tPA suspension, DOX@tPA-HP suspension and DOX@CREKA/tPA-HP suspension (the content of DOX and tPA was 20 μg and 25 μg, respectively) were placed on the top of the fibrin gel. 4 h later, the culture medium was removed, and the cells were washed with PBS for three times. After that, the cells were digested with trypsin and cellular uptake of DOX were detected using a flow cytometer (Berkman Coulter, CytoFLEX).

***In vitro* antitumor effect of DOX@CREKA/tPA-HP across fibrin gel**

To detect *in vitro* antitumor effect of DOX@CREKA/tPA-HP across fibrin gel, we performed the same procedure as it was in cellular uptake, except that 4T1 cells were incubated for 24 h after adding samples on the top of the fibrin gel. Then, *in vitro* cytotoxicity was studied by MTT assay.

Pharmacokinetics

Female BALB/c mice were randomly divided into four groups. DOX, DOX@HP, DOX@tPA-HP and DOX@CREKA/tPA-HP (4 mg kg^{-1} as DOX) were intravenously injected into mice. At pre-determined time points (0.083, 0.333, 1, 2, 4, 8, 12 and 24 h), 40 μL of plasma samples were collected. 40 μL plasma samples were mixed with 120 μL methanol and incubated in 4 °C for 1 h. Then, the mixtures were centrifuged at

15,000 rpm for 10 min, and 100 μL of the supernatants were used for DOX fluorescence determination by multimode microplate reader. The calibration curves were generated by adding increasing amounts of DOX to the blank plasma samples and the samples were treated using the same protocol as described above. Pharmacokinetic parameters were calculated according to noncompartmental model by Drug and Statistics (DAS) software.

Pharmacodynamics

4T1 tumor bearing mice models were constructed by subcutaneous injection of 1×10^6 4T1 cells in BALB/c mice. When tumor volumes reached about 50 mm^3, the mice were randomly divided into 8 groups: (1) PBS, (2) tPA, (3) DOX, (4) DOX + tPA, (5) DOX@HP, (6) DOX@HP + tPA, (7) DOX@tPA-HP, and (8) DOX@CREKA/tPA-HP. DOX, nanoparticles and tPA (4 mg kg^{-1} as DOX and 5 mg kg^{-1} as tPA) were intravenously injected at day 0, day 3, day 6 and day 9. The tumor lengths and widths were recorded every 2 days for 12 days and the tumor volume was calculated according to the following formula:

$$V = \frac{\text{length} \times \text{width}^2}{2}$$

Tumor inhibition rate (TIR) calculated by tumor volume was using the following formula:

$$TIR = 1 - \frac{V_{treament}}{V_{PBS}} \times 100\%$$

The mice were weighed every 2 days as well. At day 12, 4T1 tumor bearing mice were sacrificed and tumors were harvested for weighing. TIR calculated by tumor weight was using the following formula:

$$TIR = 1 - \frac{W_{treament}}{W_{PBS}} \times 100\%$$

The photo of tumors was taken later. Then, the tumors were fixed with 4% paraformaldehyde for hematoxylin and eosin (H&E) staining, TUNEL staining, Ki67 immunohistochemical staining, fibrin staining and CD31 staining. Simultaneously, hearts, livers, spleens, lungs, and kidneys were harvested and fixed with 4%

paraformaldehyde. H&E staining of major organ sections was performed to evaluate the adverse effects of treatments. The whole blood and serum were collected to evaluate the toxicity of treatments as well.

Survival study

4T1 tumor bearing mice were constructed as described above and drug administration was repeated without sacrificing mice. The death time of mice was recorded when mice died, or the tumor volume reached 1500 mm^3.

Evaluation of fibrin content and blood vessels

The tumors harvested from pharmacodynamics experiment were utilized to evaluate the fibrin content and blood vessels by immunofluorescence staining. The blood vessels in tumor sections were evaluated by CD31 immunofluorescence staining. The fluorescence intensity of fibrin and CD31 in tumor sections was semi-quantified by Image-Pro Plus. Vessel tortuosity (T) was calculated by the following formula:

$$T = \frac{L}{S} - 1,$$

in which L is the length of a vessel, and S is the straight-line distance between two endpoints of the vessel.[18]

Quantification of solid stress

4T1 orthotopic tumor model was established. When tumor volumes reached about 200 mm^3, the mice were randomly divided into 8 groups: (1) PBS, (2) tPA, (3) DOX, (4) DOX + tPA, (5) DOX@HP, (6) DOX@HP + tPA, (7) DOX@tPA-HP, and (8) DOX@CREKA/tPA-HP. DOX, nanoparticles and tPA (4 mg kg^{-1} as DOX and 5 mg kg^{-1} as tPA) were intravenously injected every 3 days for 4 times in total. Tumors were harvested 24 h after the last injection. Then, tumors were cut from the surface to 80% depth. After relaxing for 10 min in PBS, the tumor opening and tumor height were measured.[19, 42] The normalized tumor solid stress was calculated using the following formula:

$$\text{normalized solid stress} = \frac{\text{tumor opening}}{\text{tumor height}}$$

Evaluation of tumor stiffness

Tumor stiffness was evaluated by AFM as previously described.[43] Briefly, tumor tissues were frozen and cut into tumor slices (20 μm). Then, tumor slices were thawed in PBS at room temperature. During the measurements, tumor slices were immersed in PBS containing proteinase inhibitor. More than 500 measurements for 3 different tumors in each group were tested by AFM at room temperature. The measurement used an MSNL-10 probe with force volume model (Multi-Mode 8 AFM, Bruker, Santa Barbara, USA). The spring constant of tip is 0.01 N m^{-1} and tip radius is 20 nm. Samples were indented at a 330 nm s^{-1} loading rate, with a maximum force of 64.46 pN. The Young's modulus was calculated according to the Hertz modal. Tumor tissues were supposed to be incompressible and a Poisson's ratio of 0.5 was utilized in each calculation.

Evaluation of blood perfusion

4T1 orthotopic tumor model was established. The same operational process was carried out as it was in the "Detection of solid stress". Mice were anesthetized, and the tumor blood perfusion was tested by a PeriCam PSI System 24 h after the last administration.[18]

Drug delivery and tumor accumulation

1,1-Dioctadecyl-3,3,3,3-tetramethylindotricarbocyanine iodide (DiR) was used as a tracer to characterize the drug delivery and tumor accumulation of nanoparticles. 4T1 tumor bearing mice were constructed subcutaneously. When tumor volumes reached around 200 mm^3, the mice were randomly divided into 6 groups: (1) DiR, (2) DiR + tPA, (3) DiR@HP, (4) DiR@HP + tPA, (5) DiR@tPA-HP, and (6) DiR@CREKA/tPA-HP. DiR, DiR-loaded nanoparticles and tPA (1 mg kg^{-1} as DiR and 5 mg kg^{-1} as tPA) were intravenously injected into the mice. Then, the tumor-bearing mice were anesthetized and imaged at predetermined time points (0, 1, 2, 4, 8, 12, 24 and 48 h) using an *in vivo* imaging system with the excitation wavelength of 745 nm and the emission wavelength of 831 nm. At the end of the time point, mice were sacrificed, and major organs (hearts, livers, spleens, lungs, and kidneys) and tumors were harvested for *ex vivo* fluorescence imaging.

Statistical analysis

Experiments were repeated at least three times to obtain the mean value with standard error of mean. Statistical analysis was performed with one-way ANOVA analysis or Student's *t*-test. The differences were considered significant for $*p < 0.05$ and highly significant for $**p < 0.01$ or $***p < 0.001$. ns stands for not significant.

Results

Preparation of DOX@CREKA/tPA-HP

To co-deliver DOX and tPA to solid tumors, we synthesized an amphiphilic block polymer, PA-HES-pH-PLA. The synthetic route of PA-HES-pH-PLA is described in Fig. S1. The structure and ^{1}H NMR spectra of HES-PA, PA-HES-ALD, and PA-HES-pH-PLA are represented in Fig. S2. The new characteristic peaks appearing between 7.0-8.5 ppm illustrate the successful conjugation between PA·HCl and HES (Fig. S2A). The characteristic peaks around 10.0 ppm in Fig. S2B demonstrate that aldehyde groups have been modified to HES. PA-HES-pH-PLA is prepared by coupling hydrophilic HES with hydrophobic PLA through pH responsive Schiff base bonds. A reduction of the peaks of aldehyde groups at around 10.0 ppm and the characteristic peaks of PLA appearing between 1.40-1.50 ppm in the ^{1}H NMR spectra indicate the formation of Schiff base bonds between the PA-HES-ALD and PLA-NH_2 (Fig. S2B and S2C).[44] The degree of PLA substitution for PA-HES-pH-PLA is 1.68. The biological safety of PA-HES-pH-PLA was evaluated by using 4T1 cancer cells and 3T3 fibroblasts. High concentration of PA-HES-pH-PLA did not affect proliferation of either cancer cells or normal cells, demonstrating its biosafety (Fig. S3). This amphiphilic block polymer can self-assemble into nanoparticles and encapsulate hydrophobic drug through hydrophobic interaction. Schiff base conjugation linkage between HES and PLA is an acid-sensitive bond, which endows nanoparticles with a pH-responsive drug release function in acidic tumor microenvironment.[44, 45] PA-HES-pH-PLA can further react with cysteine-contained peptides and proteins via disulfide exchange. Therefore, CREKA and tPA can be conveniently decorated on nanoparticles. As shown in Fig. 1A, we prepared DOX@CREKA/tPA-HP in two steps. First, DOX was encapsulated in PA-HES-pH-PLA through emulsification method to afford DOX@HP. Then, tPA and

CREKA were added to DOX@HP suspension to obtain DOX@CREKA/tPA-HP. The drug loading contents of DOX and tPA in DOX@CREKA/tPA-HP are 4.18% and 5.17%, respectively. The drug loading efficiencies of DOX and tPA in DOX@CREKA/tPA-HP are 48.94% and 75.65%, respectively. In addition, the weight percentage content of CREKA in DOX@CREKA/tPA-HP is 5.23%. We also prepared DOX@HP and DOX@tPA-HP as controls. The drug loading contents and drug loading efficiencies of DOX@HP and DOX@tPA-HP are shown in Table S1.

Characterization of DOX@CREKA/tPA-HP

The hydrodynamic diameter and polydispersity index (PDI) of DOX@CREKA/tPA-HP measured by DLS are 40 nm and 0.255, respectively (Fig. 2A). TEM and AFM corroborate that DOX@CREKA/tPA-HP has a spherical morphology with a diameter around 40 nm (Fig. 2B and 2C), which agrees well with the results measured by DLS. DLS measurements further demonstrate that DOX@CREKA/tPA-HP is stable in PBS buffer (pH 7.4) for at least 7 days (Fig. 2D). The diameters of DOX@HP and DOX@tPA-HP are both around 40 nm, as measured by DLS, TEM, and AFM (Fig. S4A-S4F). In addition, both DOX@HP and DOX@tPA-HP are stable in PBS buffer via 7-day testing by DLS (Fig. S4G and S4H). When DOX@CREKA/tPA-HP, DOX@HP and DOX@tPA-HP were placed in PBS buffer containing 10% FBS, the diameters of these three nanoparticles were stable in this condition for at least 48 h (Fig. S5). These results indicate that these nanoparticles are expected to be stable *in vivo*. The ζ-potentials of these three nanoparticles were measured by DLS as well. The results in Fig. S6 show that they have near neutral surface charges. These results indicate that these three nanoparticles have similar characteristics in size, morphology, stability, and ζ-potential. With an acid-sensitive bond in DOX@CREKA/tPA-HP, we evaluated DOX release behaviors under different pH conditions. The cumulative release curve in Fig. 2E supports that more than 90% of DOX is released when DOX@CREKA/tPA-HP is in a pH 4.5 citrate buffer. In a weakly acidic PBS buffer (pH 6.5), the release percentage is 70.53%, which is 16.49% higher than that in a near neutral condition (pH 7.4). These results suggest that DOX@CREKA/tPA-HP has a pH-responsive drug release capacity. Since tPA and CREKA were decorated on the surface of nanoparticle,

we need to verify that the activities of tPA and CREKA were not affected. The enzymatic activity of tPA was detected by S-2288.[41] The relative fibrinolytic activity of tPA in DOX@CREKA/tPA-HP is 0.86 (Fig. 2F), indicating conjugating tPA on the surface of nanoparticle exerts a negligible impact on tPA activity. The fibrin targeting capability of CREKA was investigated as well. The targeting ability of CREKA was characterized by detecting the content of the residual nanoparticles on fibrin gels. Fig. S7 shows that the fluorescence intensity of DOX@CREKA/tPA-HP is 1.46 times higher than that of DOX@tPA-HP, indicating the fibrin targeting capacity of CREKA in DOX@CREKA/tPA-HP. Together, these results suggest that PA-HES-pH-PLA can load DOX and tPA and assemble into a stable and uniform pH-responsive DOX@CREKA/tPA-HP, which exhibits an excellent fibrinolytic activity and fibrin targeting capacity.

To study the penetration efficiency of DOX@CREKA/tPA-HP across fibrin matrix, an *in vitro* Transwell assay was performed. As shown in Fig. 2G, fibrin gel was prepared in the top insert of a Transwell plate. Six groups of samples were placed on the surface of fibrin gels. We analyzed the migration ability of DOX and nanoparticles by detecting the DOX fluorescence intensity in bottom wells. We found that tPA promoted the diffusion of DOX and DOX loaded nanoparticles through fibrin gel (Fig. 2H). The contents of DOX across fibrin gel in DOX+ tPA, DOX@HP + tPA, DOX@tPA-HP and DOX@CREKA/tPA-HP groups are 12.10, 12.93, 13.34 and 13.58 μg, respectively. However, in the absence of tPA, the amounts of DOX across fibrin gel in DOX and DOX@HP groups are reduced to 10.35 and 10.80 μg, respectively. This result reveals that tPA and tPA-loaded nanoparticles can promote the migration of free DOX or nanomedicine in fibrin matrix by decomposing fibrin,[22-24] implying that DOX@CREKA/tPA-HP has the potential to penetrate extracellular fibrin network and eliminate the cancer cells embedded in fibrin matrix. To validate this hypothesis, we study cellular uptake and *in vitro* antitumor effect of DOX@CREKA/tPA-HP across fibrin gel. We first analyze cellular uptake and cytotoxicity of DOX@CREKA/tPA-HP without fibrin gel. Fig. S8A and S8B show that there is no significant difference in cellular uptake among the six groups in the absence of fibrin matrix. The MTT results

in Fig. S8C also indicate a negligible difference in cytotoxicity among different groups. Next, we evaluate cellular uptake and toxicity of DOX@CREKA/tPA-HP in a fibrin gel model. The model was constructed in a Transwell plate as described in Methods and Materials. It should be noted that 4T1 cells were seeded in bottom wells. The results in Fig. 2I and 2J demonstrate that cellular uptake amounts of DOX and DOX@HP groups are decreased, as the fibrin gel forms a physical barrier that hampers the internalization of drugs by 4T1 cells. Upon decomposing fibrin via tPA, cellular uptake amounts are significantly increased. The amount of DOX in 4T1 cells for DOX + tPA group is 1.49 times higher than that in DOX group, while the cellular uptakes of nanoparticles in DOX@HP + tPA, DOX@tPA-HP and DOX@CREKA/tPA-HP groups are 1.53, 1.52 and 1.84 times as much as that in DOX@HP group (Fig. 2I and 2J). Furthermore, the result of MTT assay is consistent with that of cellular uptake. Data in Fig. 2K corroborate a significantly increased *in vitro* antitumor effect of DOX and nanoparticles as fibrin is decomposed by tPA. Together, these results demonstrate that dense fibrin hampers the diffusion of DOX and DOX-loaded nanoparticles to tumor cells in *in vitro* conditions. Decomposing fibrin can promote the penetration of DOX and nanoparticles across fibrin matrix, thereby boosting antitumor effect of DOX.

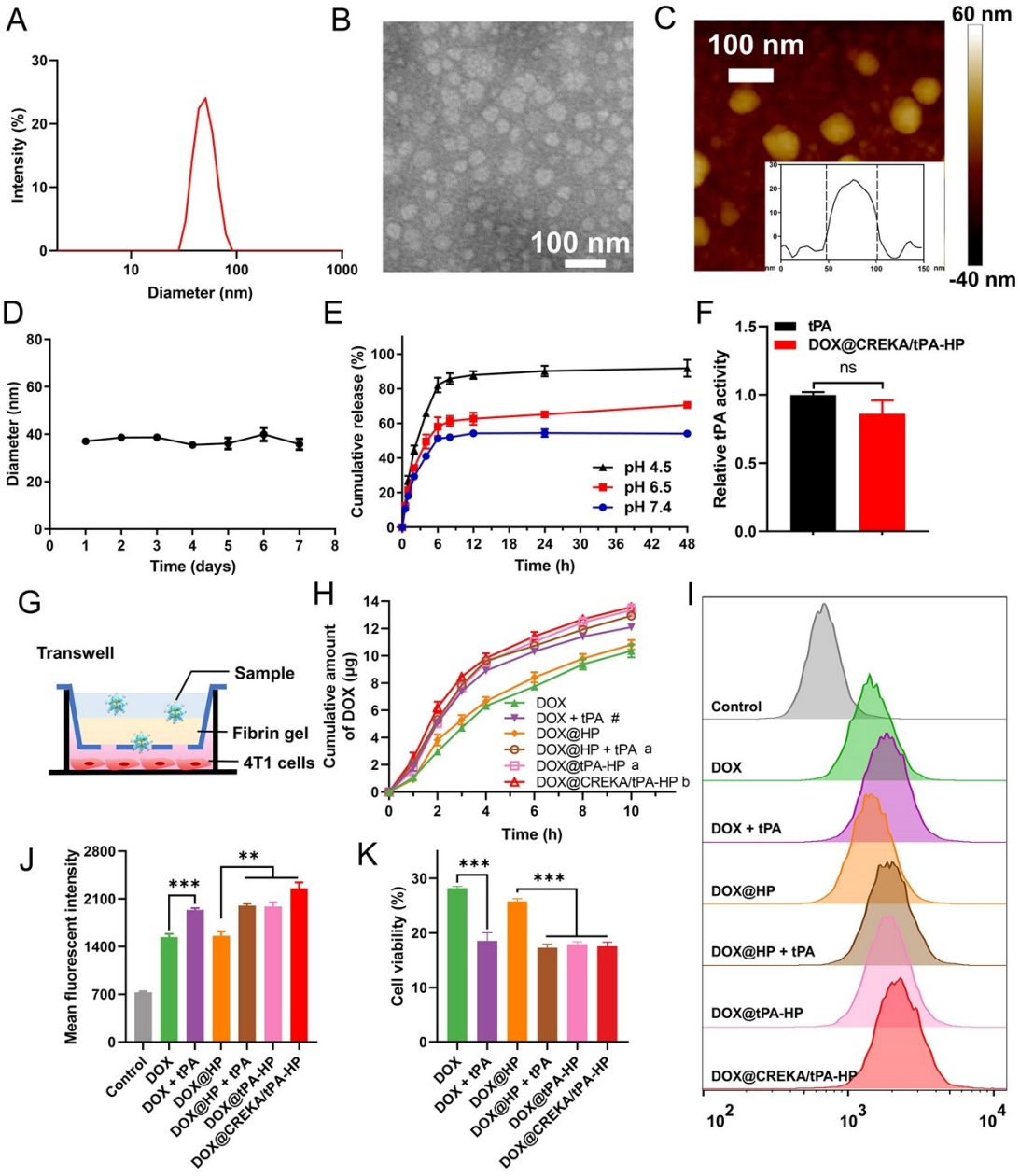

Fig. 2 Characterization of DOX@CREKA/tPA-HP. (A) Hydrodynamic diameter distribution of DOX@CREKA/tPA-HP. (B) TEM image of DOX@CREKA/tPA-HP. The scale bar is 100 nm. (C) AFM image of DOX@CREKA/tPA-HP. The scale bar is 100 nm. (D) Stability of DOX@CREKA/tPA-HP in PBS (n = 3). (E) Cumulative release of DOX under different pH conditions (n = 3). (F) Relative enzymatic activity of tPA on the surface of DOX@CREKA/tPA-HP (n = 4). (G) Evaluation of DOX@CREKA/tPA-HP across fibrin gel by Transwell assay. (H) Cumulative amount of DOX accumulated in the bottom chamber of Transwell plate over time (n = 4). # represents $p < 0.05$, relative to DOX group. a represents $p < 0.05$ and b represents $p <$

0.01, relative to DOX@HP group. (I) Cellular uptake of DOX@CREKA/tPA-HP across fibrin gel by Transwell assay and (J) its quantification (n = 4). (K) *In vitro* antitumor effect of DOX@CREKA/tPA-HP across fibrin gel after incubation for 24 h by Transwell assay (n = 6). $^{**}p < 0.01$, $^{***}p < 0.001$. ns stands for not significant. Data represent the mean ± SEM.

DOX@CREKA/tPA-HP modulates tumor stiffness by decomposing fibrin

Before we studied the biological effect of DOX@CREKA/tPA-HP, we first evaluated the pharmacokinetics of free DOX and the three DOX-loaded nanoparticles. As exhibited in Fig. S9 and Table S2, the plasma concentration in DOX group suddenly decreases to about 1.44 μg/mL at the first time point (5 min). Nevertheless, the plasma concentration in DOX@HP, DOX@tPA-HP and DOX@CREKA/tPA-HP groups at the first time point are 4.71, 3.66 and 3.43 μg/mL, respectively, demonstrating that DOX-loaded nanoparticles are more likely to be retained in plasma than distributed to tissues and organs. In addition, there are no significant differences in elimination half-life time and clearance rate among these three nanoparticles. These results illustrate that the pharmacokinetic behaviors of these three nanoparticles have little difference, which would not affect the subsequent evaluation of biological effects of these nanoparticles. To estimate the fibrin degradation effect of DOX@CREKA/tPA-HP in *in vivo* settings, 4T1 tumor-bearing mice were constructed. The mice were randomly divided into 8 groups with various treatments. Then, tumors were harvested, and the fibrin was determined by immunofluorescence staining. As illustrated in Fig. 3A, the fluorescence intensity of fibrin is significantly reduced after DOX@CREKA/tPA-HP treatment. In detail, fibrin fluorescence intensities reduce by 24.18% and 45.39% in tPA and DOX + tPA groups, respectively, relative to PBS group (Fig. 3C). Consistent with previous studies,[22-24] these results suggest that free tPA is capable of decomposing intratumoral fibrin. However, the reduction of fibrin content by using free tPA is not significant. Once tPA is delivered by nanoparticles, the fibrinolytic effect of tPA is improved owing to elevated delivery to tumors by the enhanced permeability and retention (EPR) effect.[46, 47] DOX@tPA-HP degrades around 60.04% of fibrin relative to PBS group. Nevertheless, the fibrin decomposition ability of DOX@tPA-HP is not conspicuous

when compared with DOX@HP treatment. The fibrinolytic capacity of tPA-loaded nanomedicine can be further elevated with the help of CREKA. The fibrinolytic rate of DOX@CREKA/tPA-HP group is 67.64%, which is significantly higher than that of DOX@HP group. In the absence of tPA, the fibrin contents in DOX and DOX@HP groups have negligible changes, as compared with PBS group. These results suggest that DOX@CREKA/tPA-HP can effectively eliminate intratumoral fibrin, implying that DOX@CREKA/tPA-HP possesses the potential to modulate tumor mechanics in 4T1 tumors. Consequently, we sought to study the impact of fibrin content on tumor mechanical stiffness. Young's Modulus mapping of 4T1 tumors was obtained by testing frozen tumor slices with AFM (Fig. 3B). Representative force-distance curves are displayed in Fig. S10. The mean Young's Modulus was calculated by 520 measurements from 3 samples in each group (Fig. 3D). DOX@CREKA/tPA-HP markedly reduces tumor stiffness. The mean Young's Modulus of DOX@CREKA/tPA-HP group is 2.45 kPa, which is much lower than that of PBS group (7.07 kPa) and DOX@HP group (4.52 kPa). Meanwhile, the mean modulus of DOX@tPA-HP group is 3.53 kPa, which is about half as much as that of PBS group. These results implying that tPA-induced fibrin decomposition can effectively reduce tumor stiffness. In addition, the mean modulus of DOX@CREKA/tPA-HP group is much lower than that of DOX@tPA-HP group, indicating the importance of introducing CREKA into this drug delivery system. Furthermore, there is no statistically significant difference between DOX@tPA-HP group and DOX@HP group, and DOX@CREKA/tPA-HP reduces tumor stiffness prominently when compared with DOX@HP group. This result also demonstrates the significant role of CREKA. It is important to point out that tumor stiffness is affected by not only ECM components but also tumor growth.[48] Take DOX + tPA group (2.95 kPa) and DOX@HP group (4.52 kPa) for comparison, they possess relatively lower modulus as these two groups can either decompose intratumoral fibrin to some extent[22-24] (Fig. 3A) or have a potent tumor suppression effect.[36] By contrast, the fibrinolytic effect and tumor cell killing ability are both limited in tPA group and DOX group, thus resulting in higher stiffness (tPA group: 6.76 kPa; DOX group: 7.85 kPa). Collectively, these

results corroborate that DOX@CREKA/tPA-HP significantly reduces mechanical stiffness by decomposing intratumoral fibrin in 4T1 tumors.

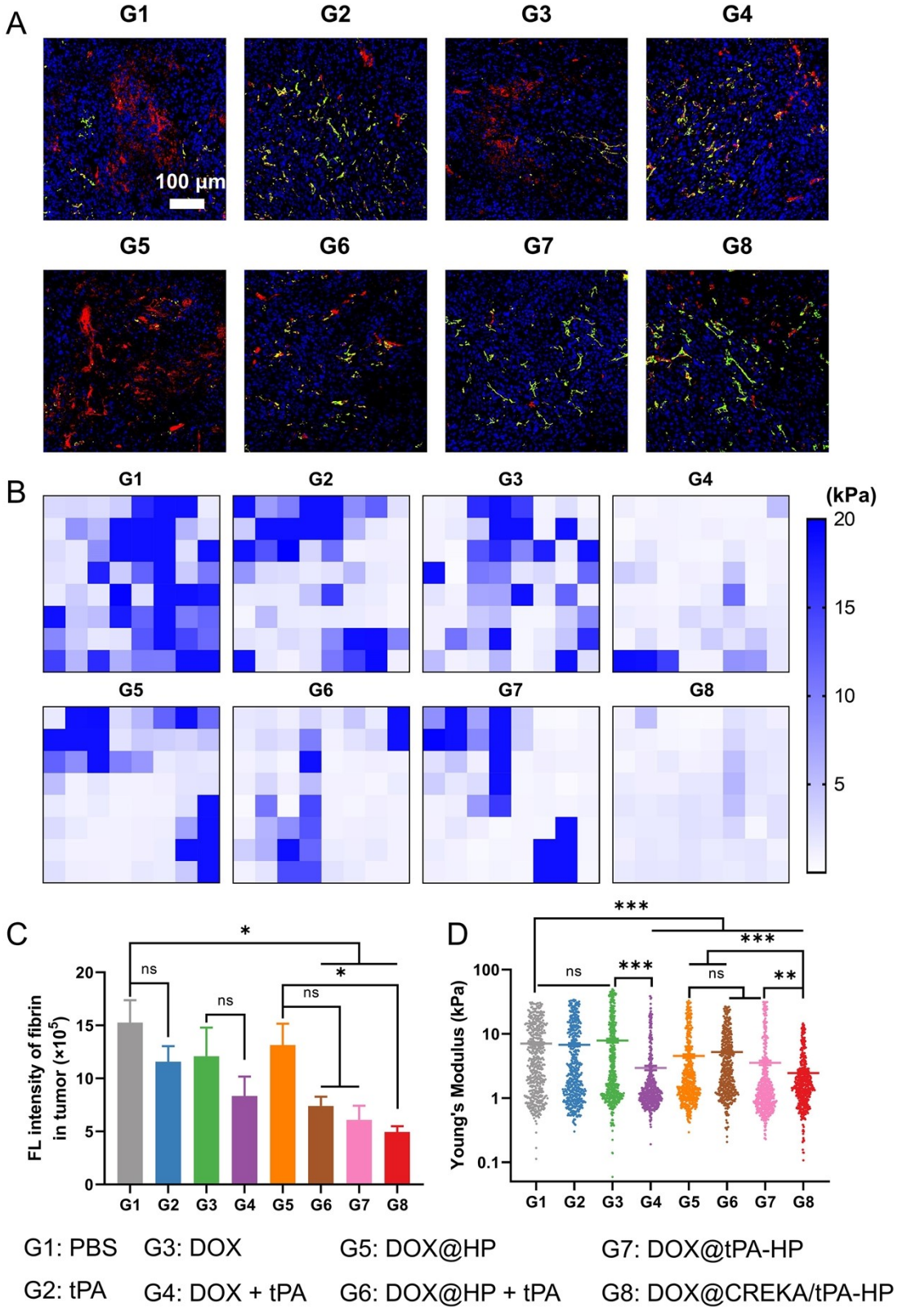

Fig. 3 DOX@CREKA/tPA-HP modulates tumor stiffness by decomposing fibrin. (A) Representative images of fibrin and CD31 in tumors by immunofluorescence

staining (red: fibrin, green: CD31, and blue: nucleus). The scale bar is 100 μm. (B) Representative tumor modulus maps of tumor slices after various treatments. (C) Quantification of fibrin fluorescence intensity in tumor sections by Image Pro Plus (n = 3 animals group^{-1}). (D) Young's Modulus of 4T1 tumor tissues after various treatments (n = 520). *$p < 0.05$, **$p < 0.01$, ***$p < 0.001$. ns stands for not significant. Data represent the mean ± SEM.

DOX@CREKA/tPA-HP reduces solid stress, decompresses blood vessels, and promotes blood perfusion

Fig. 3 demonstrates DOX@CREKA/tPA-HP significantly reduces 4T1 tumor stiffness by decomposing intratumoral fibrin. We next explored the impact of DOX@CREKA/tPA-HP on solid stress, another important mechanical parameter, which is distinguished from mechanical stiffness.[8, 48, 49] Tumor solid stress was tested by tumor opening as described in previous reports.[42, 50] Consistent with mechanical stiffness, solid stress in 4T1 tumors is dramatically declined post DOX@CREKA/tPA-HP treatment (Fig. 4A). Data in Fig. 4B show that PBS (0.475), DOX (0.511) and DOX@HP groups (0.463) have large tumor openings, indicating that high solid stresses are stored in 4T1 tumors of these groups. The normalized tumor opening of DOX@CREKA/tPA-HP group is 0.248, which is only about half of those in PBS and DOX@HP groups. Solid stress in 4T1 tumors can also be alleviated to a certain extent in other groups with tPA treatment. Specifically, the normalized tumor openings of tPA, DOX + tPA, DOX@HP + tPA and DOX@tPA-HP groups are 0.353, 0.318, 0.335, and 0.325, respectively. However, the reduction of tumor openings in these groups are inferior to that in DOX@CREKA/tPA-HP group. Fig. 4A and 4B demonstrate that DOX@CREKA/tPA-HP conspicuously reduces solid stress in 4T1 tumors. As an outcome of the reduced solid stress, the structure and function of intratumoral blood vessels might be improved.[51, 52] CD31 immunofluorescence staining results are exhibited in Fig. 3A. The density of tumor blood vessels was assessed by measuring the fluorescence intensity of CD31 within tumor tissues. As quantified in Fig. 4C, the fluorescence intensities of CD31 decrease after DOX and DOX@HP treatments. This result might be caused by DOX-induced indiscriminate damage to blood vessels.[53]

However, the fluorescence intensities of CD31 in DOX@tPA-HP group and DOX@CREKA/tPA-HP group prominently increase as compared with DOX@HP group, indicating that reduction of solid stress enhances blood vessel density. Vessel tortuosity is another important indicator reflecting the compression of tumor blood vessels. Fig. 4D shows that tumor blood vessels in PBS, DOX, and DOX@HP groups have a high tortuosity around 0.42. Notably, the tortuosity can be reduced when solid stress is alleviated. Among these 8 groups, DOX@CREKA/tPA-HP treatment achieves the lowest tortuosity (0.18), suggesting a significant decompression of intratumoral blood vessels in 4T1 tumors. To determine the function of vessels, intratumoral blood perfusion of different groups was investigated by a PeriCam PSI System (Fig. 4E). Fig. 4F reveals that DOX@CREKA/tPA-HP accomplishes the highest blood perfusion among all groups, which is increased by 39.75% as compared with PBS group. Collectively, these results confirm that DOX@CREKA/tPA-HP remarkably reduces tumor solid stress, contributing to decompressed blood vessels and promoted blood perfusion.

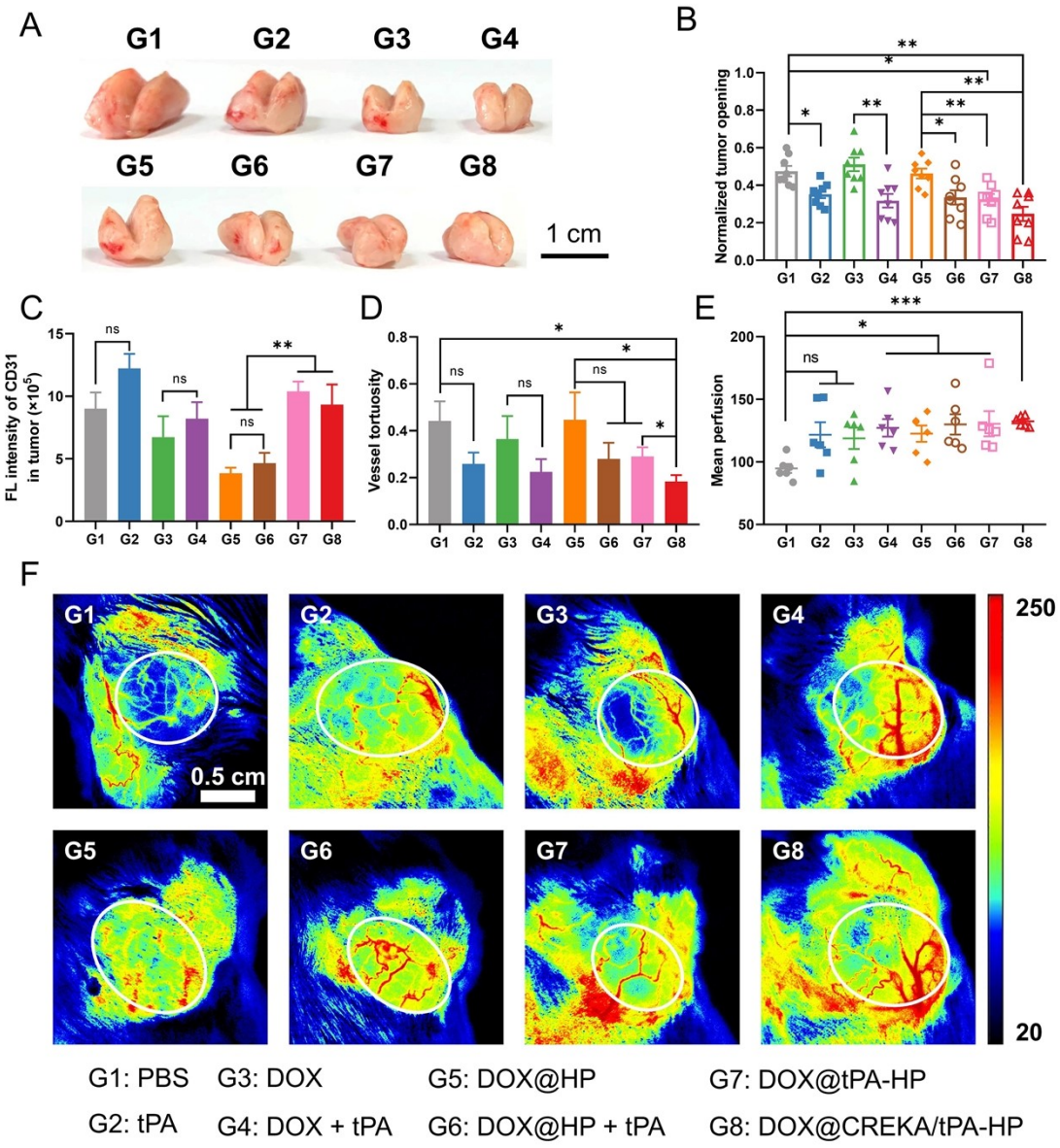

Fig. 4 DOX@CREKA/tPA-HP reduces solid stress, decompresses blood vessels, and promotes blood perfusion in 4T1 tumors. (A) Representative tumor opening in each group. The scale bar is 1 cm. (B) Normalized solid stress calculated by tumor opening divided by tumor height (n = 8). (C) CD31 fluorescence intensity in tumor sections semi-quantified by Image Pro Plus (n = 3 animals group^{-1}). (D) Tumor blood vessel tortuosity after different treatments (n = 3 animals group^{-1}). (E) Mean blood perfusion (n = 6) and (F) its representative images in each group. The white circles represent tumor regions. The scale bar is 0.5 cm. *$p < 0.05$, **$p < 0.01$, ***$p < 0.001$. ns stands for not significant. Data represent the mean ± SEM.

DOX@CREKA/tPA-HP promotes drug delivery and tumor accumulation

As DOX@CREKA/tPA-HP significantly reduces mechanical stiffness (Fig. 3), alleviates solid stress, decompresses blood vessels, and promotes blood perfusion (Fig. 4) in 4T1 tumors, we next sought to study whether this nanoparticle could augment drug delivery and tumor accumulation. DiR was loaded as a substitute of DOX in nanoparticles for ease of tracking and analyzing. *In vivo* fluorescent imaging shows that tumor accumulation of DiR-loaded nanoparticles is much higher than that of free DiR (Fig. 5A and 5D). Furthermore, tumor accumulation of DiR@CREKA/tPA-HP and DiR@tPA-HP significantly increases when compared with that of DOX@HP. Conversely, free tPA treatment has an insignificant effect on free DiR and DiR@HP, indicating that tPA decorated on nanoparticles would have a better effect on promoting drug delivery. *Ex vivo* fluorescent imaging of major organs and tumors exhibits the same results (Fig. 5B and 5E). Precisely, the tumor accumulation of DiR@CREKA/tPA-HP and DiR@tPA-HP are 1.43 and 1.26 times as much as DiR@HP. Compared to free DiR, DiR@CREKA/tPA-HP augments tumor accumulation by more than 2-fold. These results suggest that DiR@CREKA/tPA-HP significantly promotes drug delivery and tumor accumulation. Although DiR, as a fluorescent probe, is often used to track the biodistribution of nanomedicine,[35] there are still a few differences between DiR@CREKA/tPA-HP and DOX@CREKA/tPA-HP. To make the above results more convincing, we directly measured DOX contents in tumor tissues after various treatments by immunofluorescence staining (Fig. 5C and 5F). Consistently, free tPA has a paltry effect on free DOX and DOX@HP whereas DOX@CREKA/tPA-HP and DOX@tPA-HP remarkably enhance DOX accumulation in 4T1 tumors relative to DOX treatment. Although DOX@tPA-HP can effectively promote DOX delivery to tumors when compared with DOX treatment, it has limited advantages over DOX@HP treatment. However, DOX@CREKA/tPA-HP has incomparable advantages when compared with DOX and DOX@HP groups. This result suggests that CREKA with fibrin targeting capacity plays an important role in drug delivery. Together, these results substantiate that DOX@CREKA/tPA-HP-induced tumor mechanics modulation has a positive effect on drug delivery and tumor accumulation.

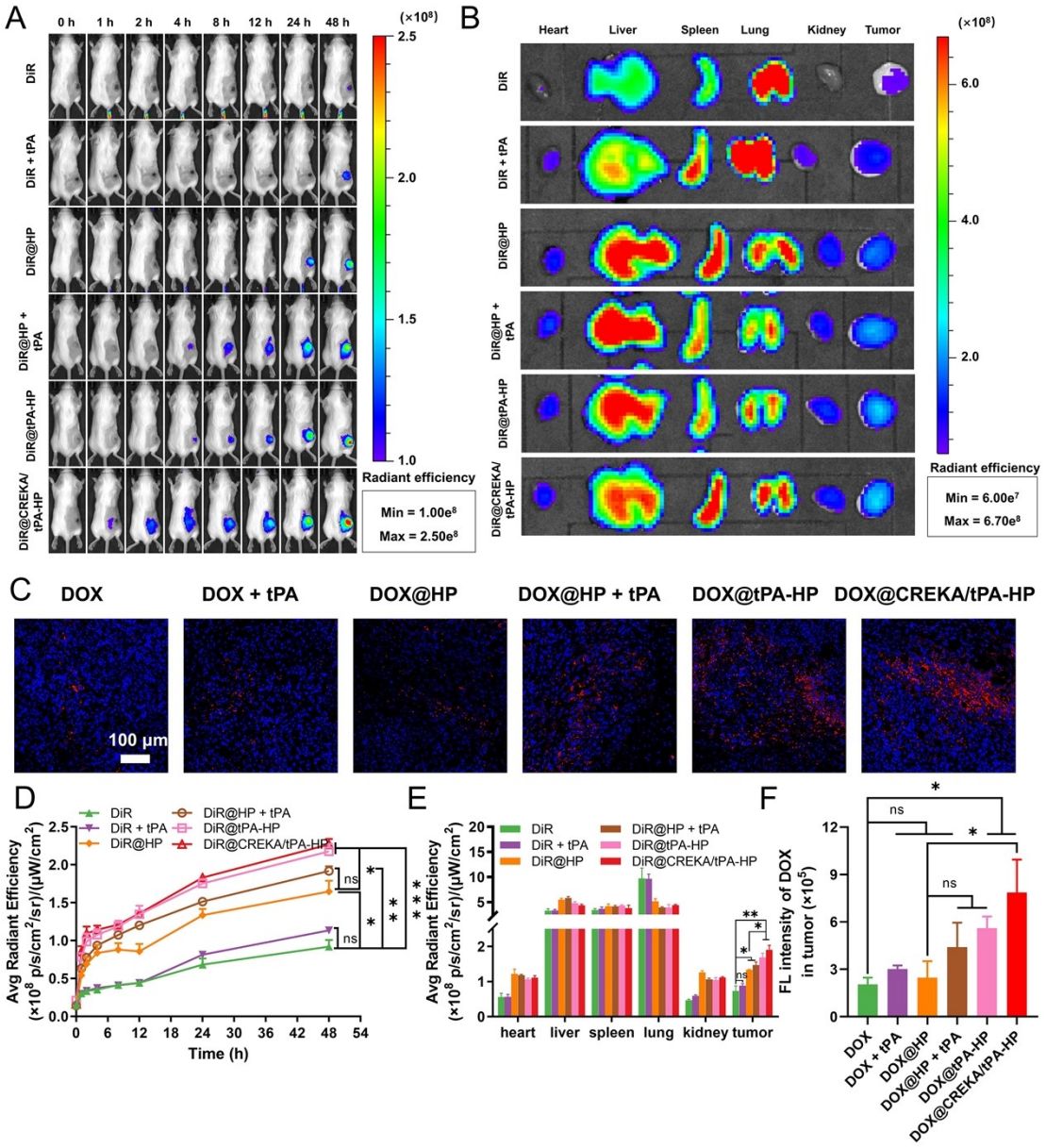

Fig. 5 DOX@CREKA/tPA-HP promotes drug delivery and tumor accumulation. (A) *In vivo* fluorescent images of 4T1 tumor bearing mice and (D) quantification of fluorescence intensity of tumors at predetermined time points (0, 1, 2, 4, 8, 12, 24 and 48 h) (n = 3). (B) *Ex vivo* fluorescent images and (E) quantification of fluorescence intensity of major organs and tumors 48 h after administration (n = 3). (C) Representative images of DOX in tumors by immunofluorescence staining (red: DOX and blue: nucleus). The scale bar is 100 μm. (F) Quantification of DOX fluorescence intensity in tumor sections by Image Pro Plus (n = 3 animals group^{-1}). *$p < 0.05$, **$p < 0.01$, ***$p < 0.001$. ns stands for not significant. Data represent the mean ± SEM.

DOX@CREKA/tPA-HP achieves potent antitumor efficacy in 4T1 tumors

Encouraged by the above results, we further used 4T1 tumor models to investigate the antitumor effects of various treatments (Fig. 6). Tumor growth curve is displayed in Fig. 6A. Tumor weight and tumor image at the end of experiment are presented in Fig. 6B and 6C. Notably, DOX@CREKA/tPA-HP exhibits the best tumor suppression effect among all eight groups. The final TIR of DOX@CREKA/tPA-HP are 60.44% and 62.02% calculated by tumor volume (Fig. 6A) and tumor weight (Fig. 6B), respectively. Compared to DOX@HP treatment, TIRs of DOX@CREKA/tPA-HP group are significantly elevated by 17.12% and 25.13%, as calculated by tumor volume and tumor weight, respectively. Furthermore, the immunohistochemical data come to the consistent conclusion (Fig. 6D). The detailed necrotic area, percentage of TUNEL positive cells and Ki67 positive cells analysis are exhibited in Fig. S11-S13. These results show that DOX@CREKA/tPA-HP treatment exhibits more necrosis by H&E staining and more apoptosis by TUNEL assay than all other groups. Ki67 assay shows that DOX@CREKA/tPA-HP treatment has a limited effect on cancer cells proliferation. Taken together, these results indicate that modulating tumor mechanics for enhanced tumor accumulation can ultimately augment antitumor efficacy.

Fig. 6 demonstrates that DOX@CREKA/tPA-HP has an optimum TIR. As a result, DOX@CREKA/tPA-HP treatment might prolong mice survival. The median survival time of DOX@CREKA/tPA-HP group is 47.5 days, which is 8.5 days longer than that of PBS group and 2 days longer than that of DOX@HP group (Fig. S14). Lung metastasis is a major factor that threaten breast cancer patients' lives. We therefore evaluated lung metastasis 25 days post various treatments by H&E staining (Fig. S15A). The metastatic area of DOX@CREKA/tPA-HP group is much lower than that of PBS group (Fig. S15B), implying that DOX@CREKA/tPA-HP can effectively reduce lung metastasis.

Severe side effects are big issues for chemotherapy. The body weights of 4T1 tumor-bearing mice were utilized to evaluate the systemic toxicity. As illustrated in Fig. S16, tPA treatment results in negligible effect on body weights. At the end of pharmacodynamic experiment, body weights in DOX group and DOX + tPA group reduce to 93% of original weights, whereas body weights in DOX-loaded nanoparticles

groups (DOX@HP, DOX@HP + tPA, DOX@tPA-HP and DOX@CREKA/tPA-HP groups) only reduce to about 97%, indicating no serious systemic adverse effects associated with these nanotherapeutic treatments. H&E staining of major organs were used to estimate toxicity of various treatments as well. For DOX and DOX + tPA groups, Fig. S17 shows obvious lesions in heart sections. For other groups, there are no evident lesions in all major organs. Moreover, the numbers of white blood cells, red blood cells, and platelets from 4T1 tumor-bearing mice post various treatments are within normal range (Fig. S18A-S18C). Alanine aminotransferase (ALT), aspartate aminotransferase (AST), blood urea nitrogen (BUN), creatinine (CREA) and creatine kinase (CK) in the serum are all in the acceptable range as well (Fig. S18D-S18H). These results corroborate that DOX@CREKA/tPA-HP augments antitumor efficacy with reduced adverse effects.

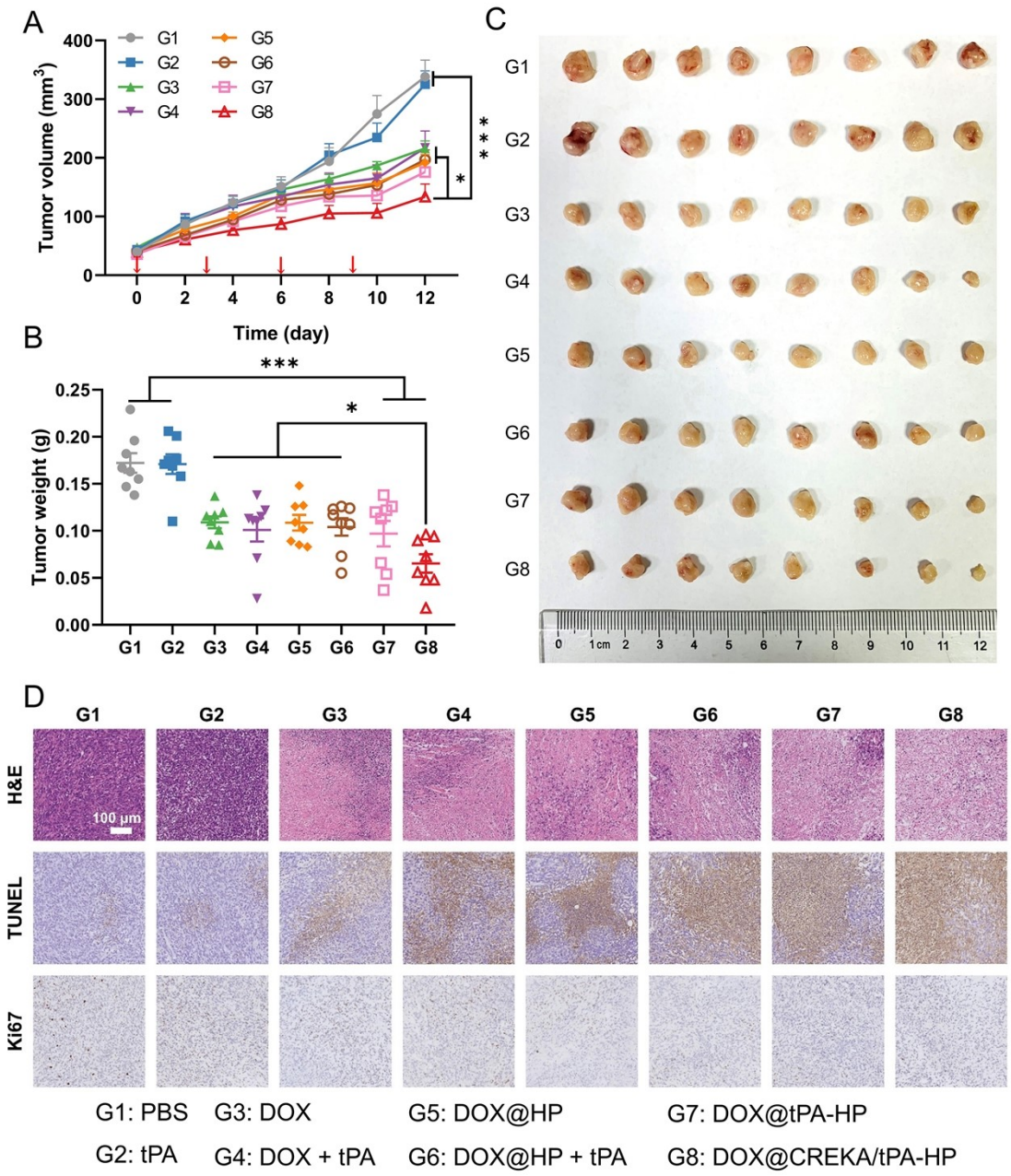

Fig. 6 DOX@CREKA/tPA-HP achieves potent antitumor efficacy in 4T1 tumors. (A) Tumor growth curve and (B) tumor weight of 4T1 tumor-bearing mice. Red arrows represent intravenous administration of drug (n = 8). (C) Image of tumors at the end of the experiment. (D) H&E staining, TUNEL and Ki67 immunohistochemistry of tumor sections at the end of the *in vivo* antitumor experiment. The scale bar is 100 μm. *p < 0.05, ***p < 0.001. Data represent the mean ± SEM.

Discussion

Abnormal tumor mechanics is a common trait for numerous solid tumors, including HCC, PDAC, and TNBC.[54] As the aberrant mechanical properties including high mechanical stiffness and solid stress have been recognized as the paramount factors that promote tumor growth,[55, 56] accelerate tumor metastasis,[57, 58] and impair drug delivery,[20] it is of significance to modulate tumor mechanics for potent cancer therapy.

To regulate the abnormal tumor mechanics and augment antitumor efficacy, here we rationally designed and successfully prepared a smart nanomedicine, DOX@CREKA/tPA-HP, with the following advantages. First, DOX@CREKA/tPA-HP can precisely modulate tumor mechanics by decomposing fibrin (Fig. 1). In detail, DOX@CREKA/tPA-HP can be accurately delivered to intratumoral fibrin region by the fibrin targeting effect of CREKA.[37, 38] Then, DOX@CREKA/tPA-HP disassembles, and DOX and tPA are released in weakly acidic tumor microenvironment. The released tPA decomposes fibrin by activating plasminogen to plasmin (Fig. 3A and 3C),[59, 60] thereby precisely modulating tumor mechanics (Fig. 3B, 3D, 4A and 4B) for improved blood perfusion (Fig. 4E and 4F), enhanced drug delivery efficiency (Fig. 5), and augmented antitumor efficacy (Fig. 6). Second, DOX@CREKA/tPA-HP not only achieves potent inhibition in primary 4T1 tumors but more importantly significantly suppresses tumor metastasis in lung (Fig. S15). The inhibition of tumor metastasis by DOX@CREKA/tPA-HP can be mainly ascribed to the following reasons. Effectively suppressing primary tumor growth by DOX@CREKA/tPA-HP can directly suppress metastasis. Moreover, the formation of lung metastasis is highly dependent on mechanical niches in lung tissues, and elimination of fibrin can impair the colonization and growth of tumor repopulating cells.[61] Third, DOX@CREKA/tPA-HP is an instructive nanoplatform for clinical cancer treatments. tPA is widely used for thrombolysis in clinical practice.[60] The combination of cancer treatments with fibrinolytic therapies in patients has been reported before.[62, 63] Therefore, it is feasible to modulate tumor mechanical properties by utilizing tPA in clinical settings when the risks and benefits are well balanced. In addition, HES and PLA are biocompatible materials.[64, 65] Our previous studies have demonstrated that HES based nanomedicines

significantly augment antitumor effect and reduce adverse effects of chemotherapeutic drugs by enhanced drug delivery to tumor tissues and decreased accumulation within major organs.[34, 35, 66] For instance, administration of DOX and LY2157299 (LY) co-loaded HES-PLA nanoparticles (DOX/LY@HES-PLA) remarkably enhanced TIR by about 25.7% and significantly reduced systemic toxicity and cardiotoxicity, as compared with free DOX treatment.[36] In current study, DOX@CREKA/tPA-HP elevates antitumor efficiency by 25.35%, relative to free DOX treatment (Fig. 6B). No serious adverse effects were observed in 4T1 tumor models during DOX@CREKA/tPA-HP treatment (Fig. S16-S18). These facts indicate that precise regulation of tumor mechanics by DOX@CREKA/tPA-HP might promote antitumor effect without imposing a great burden on patients. However, the shortcomings of this nanomedicine should be overcome before it is used in clinics. First, the pH responsive property of this nanomedicine is not sensitive enough. *In vitro* experiments demonstrate that around 40% of DOX was released in a condition with pH 7.4 (Fig. 2E). Premature leakage of DOX would be detrimental to antitumor effect. More sensitive pH-responsive bonds should be introduced to this formulation. Second, the preparation of this nanomedicine is complicated, which poses a big challenge to batch stability and mass production. It is necessary to simplify the preparation process while ensuring the effectiveness of nanomedicine. Third, this formulation is effective in improving the drug delivery efficiency, but cannot address the inherent shortcomings of chemotherapeutic drugs. It is worth pointing out that single chemotherapy can hardly eliminate cancer cells. For chemo-resistant cancer cells, this formulation can only bring limited benefits by improving drug delivery. To eradicate cancer cells, this nanomedicine should be utilized in combination with other effective antitumor strategies, including immunotherapy, radiotherapy, photothermal therapy and photodynamic therapy. Overall, DOX@CREKA/tPA-HP can prominently enhance the efficiency of chemotherapy by modulating tumor mechanical microenvironment, but it calls for further optimization for clinical applications.

In the present study, we established a direct relationship between intratumoral fibrin and aberrant tumor mechanics. DOX@CREKA/tPA-HP effectively decreases

intratumoral fibrin in 4T1 tumors by 67.64% relative to PBS group (Fig. 3A and 3C). By decomposing intratumoral fibrin, DOX@CREKA/tPA-HP conspicuously reduces mechanical stiffness and solid stress. In detail, tumor stiffness and solid stress in DOX@CREKA/tPA-HP group decrease by 65.27% and 47.79% when compared with PBS group, respectively (Fig. 3D and 4B). Previous studies have reported the strategy of leveraging tPA for enhanced drug delivery and augmented antitumor efficacy. These studies have documented the decompression of blood vessels and improved blood perfusion post elimination of fibrin by tPA in xenograft subcutaneous A549 tumor models.[22, 23] Some studies have also reported the benefits of loading tPA in nanoplatforms.[24, 67] However, the change of tumor mechanics in response to fibrin decomposition had not been explored. Herein, we, for the first time, confirmed the correlation between fibrin reduction and tumor mechanics modulation, and illustrated that both tumor blood perfusion and drug delivery were boosted by regulating tumor mechanical properties.

By decreasing solid stress (Fig. 4A and 4B), DOX@CREKA/tPA-HP significantly improves structure and function of intratumoral blood vessels in 4T1 tumor tissues (Fig. 4C-4F), thereby promoting drug delivery efficiency (Fig. 5). In the current study, free tPA and tPA-loaded nanoparticles all remarkably reduce solid stress (Fig. 4A and 4B). However, DOX@CREKA/tPA-HP has the greatest capacity for reduction of solid stress among all groups. Data show that DOX@CREKA/tPA-HP extremely decreases solid stress, compared with PBS and DOX@HP treatment ($p < 0.01$). As the result of reduced solid stress, DOX@CREKA/tPA-HP significantly decreases vessel tortuosity by 58.32% (Fig. 4D) and enhances blood perfusion by 39.75% (Fig. 4E and 4F), as compared with PBS group. Finally, DOX@CREKA/tPA-HP treatment leads to an enhanced drug delivery. DOX accumulation in 4T1 tumors of DOX@CREKA/tPA-HP group is 3.18 and 3.84 folds higher than that of DOX@HP and DOX groups, respectively (Fig. 5C and 5F). In recent years, several studies emphasize the importance of alleviating tumor solid stress in cancer therapy[68] and indicate that compression of tumor blood vessels is indeed caused by solid stress.[69] Our previous studies demonstrated that reducing solid stress through decreasing collagen and fibronectin by

HBO could promote blood perfusion and facilitate delivery of PD-1 antibody and commercial nanomedicine in murine HCC H22 tumors and TNBC 4T1 tumors, respectively.[18, 19] Reducing solid stress through inhibiting collagen synthesis by TGFβ inhibitor, LY2157299, can also decompress blood vessels and promote nanomedicine delivery in TNBC 4T1 tumors.[52] Besides, alleviating solid stress through down-regulating collagen I and HA by losartan is beneficial to restoration of vascular function and drug delivery in PDAC tumor models.[20] Down-regulating collagen and HA levels by Tranilast in primary breast cancer or breast cancer lung metastases leads to a reduction of solid stress, thereby prominently increasing blood perfusion.[50, 70] Among these researches, HBO assisted anti-PD-1 therapy in HCC patients (NCT05031949) and losartan combined chemotherapy for pancreatic cancer (NCT01821729) are currently undergoing clinical trials. These studies collectively demonstrate that decreasing ECM components including collagen, HA, and fibronectin significantly reduces solid stress, and the reduction of solid stress is conducive to drug delivery. However, the role of fibrin, a vital ECM component, on solid stress is unclear thus far. By reducing solid stress via DOX@CREKA/tPA-HP treatment in TNBC 4T1 tumor models, we, for the first time, reveal that fibrin can be a new target for solid stress mitigation. Therefore, this study provides a new method to alleviate aberrant solid stress, promote blood perfusion, and boost drug delivery for potent cancer therapy.

Regulating tumor mechanical stiffness is fundamental to cancer therapy. In the present study, DOX@CREKA/tPA-HP effectively reduces tumor stiffness. Compared with PBS, tPA and DOX@HP groups, the mean Young's Modulus of tumor tissues in DOX@CREKA/tPA-HP group decreases by 65.27%, 63.67% and 45.71%, respectively (Fig. 3D). However, the effect of reduced mechanical stiffness on tumor physiology is controversial. One view holds that cancer cells softening can increase the invasion and metastasis potential,[71] and the relatively soft mechanical microenvironment promotes the growth of tumor repopulating cells.[72] The opposite view deems that a stiff microenvironment is highly correlated with malignancy degree.[73-75] Tumor stiffening is believed to promote tumor progression including accelerating tumor invasion and metastasis,[57, 58] enhancing cancer stemness,[56] inducing

epithelial-mesenchymal transition,[76] altering tumor metabolism,[77] and increasing angiogenesis and vessel permeability.[78] Whether tumor progression and metastasis require a soft mechanical microenvironment or a stiff mechanical microenvironment remains to be elucidated further. Nevertheless, the reduction of mechanical stiffness is thought to be beneficial to drug delivery.[16, 79] Therefore, reducing tumor stiffness by DOX@CREKA/tPA-HP for subsequent drug delivery appears to be important. As the growth of cancer stem cells (CSCs) depends on the mechanical stiffness of fibrin gels,[72] decomposing intratumoral fibrin by DOX@CREKA/tPA-HP might have a potential effect on decreasing CSCs. This conjecture has not been studied in the current research, whereas eliminating CSCs by modulating tumor stiffness is quite interesting and needs further study.

Conclusion

In this study, we prepared a neotype smart nanomedicine, DOX@CREKA/tPA-HP, with precise fibrin decomposition and tumor mechanics modulation capacities. *In vitro* Transwell assays showed that DOX@CREKA/tPA-HP could effectively diffuse in fibrin matrix by decomposing fibrin, thus leading to an enhanced cellular uptake and elevated antitumor effect. *In vivo* experiments exhibited that DOX@CREKA/tPA-HP significantly reduced intratumoral fibrin contents and regulated tumor mechanical properties, thereby decompressing blood vessels, elevating blood perfusion, promoting drug delivery, and finally augmenting chemotherapeutic effect. These findings have the following critical implications. First, DOX@CREKA/tPA-HP could precisely modulate tumor mechanics for potent cancer therapy, which might be an instructive nanomedicine for further designing a series of smart nanomedicines with accurate tumor mechanics modulation capacity. Second, we elucidated a relationship between fibrin content and mechanical properties and demonstrated that intratumoral fibrin was a new target for regulating tumor mechanics. Third, this study raises some interesting questions for further research. Limited by existing technology, the present study lacks valid method to specifically quantify the stress applied to intratumoral blood vessels. Therefore, the relationship between tumor mechanics and vascular requires further

studies. Besides, molecular signaling pathways are closely related to tumor mechanics. The downstream signaling pathways and the relevant biological effects induced by modulated tumor mechanics await further explorations.

Supporting information

The Supporting information is available free of charge.

Detailed materials and methods; synthetic steps of PA-HES-pH-PLA; ^{1}H NMR spectra of HES-PA, PA-HES-ALD, and PA-HES-pH-PLA; characterization of DOX@HP and DOX@tPA-HP; fibrin targeting assay of DOX@CREKA/tPA-HP; cellular uptake and cytotoxicity of DOX@CREKA/tPA-HP; pharmacokinetics results; typical force curves; detailed quantitative results of tumor necrotic area, TUNEL and Ki67 positive cells; survival curve; body weight curve; H&E staining of major organs; and biocompatibility assay of various treatments.

Author contributions

Z. F. Li, J. T. Chen, and X. L. Yang conceived and designed the project. J. T. Chen, Z. J. Zhang, Y. N. Li, H. W. Zeng, Z. Li, C. Wang, C. Xu, and Q. Y. Deng performed the experiments. J. T. Chen, and Z. F. Li analyzed and interpreted the data, and wrote the manuscript. Z. F. Li and X. L. Yang acquired fundings and supervised the project. J. T. Chen prepared the first draft. J. T. Chen, Z. J. Zhang, Y. N. Li, Q. Wang, and Z. F. Li reviewed and modified the manuscript. All authors discussed the results and commented on the manuscript.

Conflicts of interest

The authors (Z. F. Li, X. L. Yang, and J. T. Chen) have applied for patents related to this study.

Acknowledgement

We thank the Research Core Facilities for College of Life Science and Technology in Huazhong University of Science and Technology (HUST) and the Analytical and Testing Center of HUST for the facility support. This work was financially supported by grants from the National Research and Development Program of China (2018YFA0208900, 2020YFA0211200, and 2020YFA0710700), the National Science Foundation of China (82172757, 31972927), the Scientific Research Foundation of

Huazhong University of Science and Technology (3004170130), the Program for HUST Academic Frontier Youth Team (2018QYTD01), and the HCP Program for HUST.

Data availability statement

The data that support the findings of this study are available from the corresponding author upon reasonable request.

References

1. Y. Jiang, H. Zhang, J. Wang, Y. Liu, T. Luo and H. Hua, *J. Hematol. Oncol.*, 2022, **15**, 34.
2. B. Piersma, M. K. Hayward and V. M. Weaver, *Biochim. Biophys. Acta Rev. Cancer*, 2020, **1873**, 188356.
3. W. Zheng, Z. G. Zhou, C. H. Wong, X. Q. Pei, S. L. Zhuang, Q. Li, M. S. Chen, A. H. Li and F. J. Zhang, *Eur. Radiol.*, 2019, **29**, 1479-1488.
4. J. Riegler, Y. Labyed, S. Rosenzweig, V. Javinal, A. Castiglioni, C. X. Dominguez, J. E. Long, Q. Li, W. Sandoval, M. R. Junttila, S. J. Turley, J. Schartner and R. A. D. Carano, *Clin. Cancer Res.*, 2018, **24**, 4455-4467.
5. J. Hu, J. Guo, Y. Pei, P. Hu, M. Li, I. Sack and W. Li, *Front. Oncol.*, 2021, **11**, 701336.
6. T. Takamura, U. Motosugi, M. Ogiwara, Y. Sasaki, K. J. Glaser, R. L. Ehman, H. Kinouchi and H. Onishi, *Am. J. Neuroradiol.*, 2021, **42**, 1216-1222.
7. H. Mohammadi and E. Sahai, *Nat. Cell Biol.*, 2018, **20**, 766-774.
8. H. T. Nia, H. Liu, G. Seano, M. Datta, D. Jones, N. Rahbari, J. Incio, V. P. Chauhan, K. Jung, J. D. Martin, V. Askoxylakis, T. P. Padera, D. Fukumura, Y. Boucher, F. J. Hornicek, A. J. Grodzinsky, J. W. Baish, L. L. Munn and R. K. Jain, *Nat. Biomed. Eng.*, 2016, **1**, 0004.
9. M. Jang, J. An, S. W. Oh, J. Y. Lim, J. Kim, J. K. Choi, J. H. Cheong and P. Kim, *Nat. Biomed. Eng.*, 2021, **5**, 114-123.
10. M. Kalli and T. Stylianopoulos, *Front. Oncol.*, 2018, **8**, 55.
11. V. Gkretsi and T. Stylianopoulos, *Front. Oncol.*, 2018, **8**, 145.
12. R. Reuten, S. Zendehroud, M. Nicolau, L. Fleischhauer, A. Laitala, S. Kiderlen, D. Nikodemus, L. Wullkopf, S. R. Nielsen, S. McNeilly, C. Prein, M. Rafaeva, E. M. Schoof, B. Furtwangler, B. T. Porse, H. Kim, K. J. Won, S. Sudhop, K. W. Zornhagen, F. Suhr, E. Maniati, O. M. T. Pearce, M. Koch, L. B. Oddershede, T. Van Agtmael, C. D. Madsen, A. E. Mayorca-Guiliani, W. Bloch, R. R. Netz, H. Clausen-Schaumann and J. T. Erler, *Nat. Mater.*, 2021, **20**, 892-903.

13. H. Zhang, F. Lin, J. Huang and C. Xiong, *Acta Biomater.*, 2020, **106**, 181-192.
14. C. Liu, M. Li, Z. X. Dong, D. Jiang, X. Li, S. Lin, D. Chen, X. Zou, X. D. Zhang and G. D. Luker, *Acta Biomater.*, 2021, **131**, 326-340.
15. M. J. Mitchell, R. K. Jain and R. Langer, *Nat. Rev. Cancer*, 2017, **17**, 659-675.
16. R. K. Jain, J. D. Martin and T. Stylianopoulos, *Annu. Rev. Biomed. Eng.*, 2014, **16**, 321-346.
17. X. Wang, N. Ye, C. Xu, C. Xiao, Z. Zhang, Q. Deng, S. Li, J. Li, Z. Li and X. Yang, *Nano Today*, 2022, **44**, 101458.
18. X. Liu, N. B. Ye, C. Xiao, X. X. Wang, S. Y. Li, Y. H. Deng, X. Q. Yang, Z. F. Li and X. L. Yang, *Nano Today*, 2021, **40**, 101248.
19. X. Liu, N. B. Ye, S. Liu, J. K. Guan, Q. Y. Deng, Z. J. Zhang, C. Xiao, Z. Y. Ding, B. X. Zhang, X. P. Chen, Z. F. Li and X. L. Yang, *Adv. Sci.*, 2021, **8**, 2100233.
20. V. P. Chauhan, J. D. Martin, H. Liu, D. A. Lacorre, S. R. Jain, S. V. Kozin, T. Stylianopoulos, A. S. Mousa, X. Han, P. Adstamongkonkul, Z. Popovic, P. Huang, M. G. Bawendi, Y. Boucher and R. K. Jain, *Nat. Commun.*, 2013, **4**, 2516.
21. Y. A. Zhong, J. G. Zhang, J. M. Zhang, Y. Hou, E. P. Chen, D. C. Huang, W. Chen and R. Haag, *Adv. Funct. Mater.*, 2021, **31**, 2007544.
22. B. Zhang, T. Jiang, X. She, S. Shen, S. Wang, J. Deng, W. Shi, H. Mei, Y. Hu, Z. Pang and X. Jiang, *Biomaterials*, 2016, **96**, 63-71.
23. A. R. Kirtane, T. Sadhukha, H. Kim, V. Khanna, B. Koniar and J. Panyam, *Cancer Res.*, 2017, **77**, 1465-1475.
24. T. Mei, B. Shashni, H. Maeda and Y. Nagasaki, *Biomaterials*, 2020, **259**, 120290.
25. D. W. Zheng, S. Hong, Q. L. Zhang, X. Dong, P. Pan, W. F. Song, W. Song, S. X. Cheng and X. Z. Zhang, *Nat. Commun.*, 2020, **11**, 4907.
26. A. Falanga, L. Russo and C. Verzeroli, *Thromb. Res.*, 2013, **131**, S59-S62.
27. Z. F. Li, C. Z. Di, S. P. Li, X. L. Yang and G. J. Nie, *Accounts Chem. Res.*, 2019, **52**, 2703-2712.

28. A. Metelli, B. X. Wu, B. Riesenberg, S. Guglietta, J. D. Huck, C. Mills, A. Li, S. Rachidi, C. Krieg, M. P. Rubinstein, D. T. Gewirth, S. Sun, M. B. Lilly, A. H. Wahlquist, D. P. Carbone, Y. Yang, B. Liu and Z. Li, *Sci. Transl. Med.*, 2020, **12**, eaay4860.

29. J. S. Palumbo, K. E. Talmage, J. V. Massari, C. M. La Jeunesse, M. J. Flick, K. W. Kombrinck, M. Jirouskova and J. L. Degen, *Blood*, 2005, **105**, 178-185.

30. H. C. Kwaan and P. F. Lindholm, *Semin. Thromb. Hemost.*, 2019, **45**, 413-422.

31. X. Y. Wang, K. Tsuji, S. R. Lee, M. M. Ning, K. L. Furie, A. M. Buchan and E. H. Lo, *Stroke*, 2004, **35**, 2726-2730.

32. H. M. Wang, H. Hu, H. Yang and Z. F. Li, *RSC Adv.*, 2021, **11**, 3226-3240.

33. J. K. Guan, Y. X. Wu, X. Liu, H. M. Wang, N. B. Ye, Z. Li, C. Xiao, Z. J. Zhang, Z. F. Li and X. L. Yang, *Biomaterials*, 2021, **279**.

34. Y. H. Li, H. Hu, Q. Zhou, Y. X. Ao, C. Xiao, J. L. Wan, Y. Wan, H. B. Xu, Z. F. Li and X. L. Yang, *ACS Appl. Mater. Inter.*, 2017, **9**, 19215-19230.

35. Y. H. Li, Y. X. Wu, J. T. Chen, J. L. Wan, C. Xiao, J. K. Guan, X. L. Song, S. Y. Li, M. M. Zhang, H. C. Cui, T. T. Li, X. Q. Yang, Z. F. Li and X. L. Yang, *Nano Lett.*, 2019, **19**, 5806-5817.

36. Q. Zhou, Y. H. Li, Y. H. Zhu, C. Yu, H. B. Jia, B. H. Bao, H. Hu, C. Xiao, J. Q. Zhang, X. F. Zeng, Y. Wan, H. B. Xu, Z. F. Li and X. L. Yang, *J. Control. Release*, 2018, **275**, 67-77.

37. D. Simberg, T. Duza, J. H. Park, M. Essler, J. Pilch, L. L. Zhang, A. M. Derfus, M. Yang, R. M. Hoffman, S. Bhatia, M. J. Sailor and E. Ruoslahti, *Proc. Natl. Acad. Sci. U. S. A.*, 2007, **104**, 932-936.

38. Y. Li, X. Zhao, X. L. Liu, K. M. Cheng, X. X. Han, Y. L. Zhang, H. Min, G. N. Liu, J. C. Xu, J. Shi, H. Qin, H. M. Fan, L. Ren and G. J. Nie, *Adv. Mater.*, 2020, **32**, 1906799.

39. H. Hu, J. L. Wan, X. T. Huang, Y. X. Tang, C. Xiao, H. B. Xu, X. L. Yang and Z. F. Li, *Nanoscale*, 2018, **10**, 10514-10527.

40. H. L. Wu, H. Hu, J. L. Wan, Y. M. Li, Y. X. Wu, Y. X. Tang, C. Xiao, H. B. Xu, X. L. Yang and Z. F. Li, *Chem. Eng. J.*, 2018, **349**, 129-145.

41. J. N. Marsh, G. Hu, M. J. Scott, H. Zhang, M. J. Goette, P. J. Gaffney, S. D. Caruthers, S. A. Wickline, D. Abendschein and G. M. Lanza, *Nanomedicine*, 2011, **6**, 605-615.

42. T. Stylianopoulos, J. D. Martin, V. P. Chauhan, S. R. Jain, B. Diop-Frimpong, N. Bardeesy, B. L. Smith, C. R. Ferrone, F. J. Hornicek, Y. Boucher, L. L. Munn and R. K. Jain, *Proc. Natl. Acad. Sci. U. S. A.*, 2012, **109**, 15101-15108.

43. H. Laklai, Y. A. Miroshnikova, M. W. Pickup, E. A. Collisson, G. E. Kim, A. S. Barrett, R. C. Hill, J. N. Lakins, D. D. Schlaepfer, J. K. Mouw, V. S. LeBleu, N. Roy, S. V. Novitskiy, J. S. Johansen, V. Poli, R. Kalluri, C. A. Iacobuzio-Donahue, L. D. Wood, M. Hebrok, K. Hansen, H. L. Moses and V. M. Weaver, *Nat. Med.*, 2016, **22**, 497-505.

44. A. E. Dunn, D. J. Dunn, A. Macmillan, R. Whan, T. Stait-Gardner, W. S. Price, M. Lim and C. Boyer, *Polym. Chem.*, 2014, **5**, 3311-3315.

45. Y. Yu, C. K. Chen, W. C. Law, E. Weinheimer, S. Sengupta, P. N. Prasad and C. Cheng, *Biomacromolecules*, 2014, **15**, 524-532.

46. L. E. Gerlowski and R. K. Jain, *Microvasc. Res.*, 1986, **31**, 288-305.

47. Y. Matsumura and H. Maeda, *Cancer Res.*, 1986, **46**, 6387-6392.

48. G. Seano, H. T. Nia, K. E. Emblem, M. Datta, J. Ren, S. Krishnan, J. Kloepper, M. C. Pinho, W. W. Ho, M. Ghosh, V. Askoxylakis, G. B. Ferraro, L. Riedemann, E. R. Gerstner, T. T. Batchelor, P. Y. Wen, N. U. Lin, A. J. Grodzinsky, D. Fukumura, P. Huang, J. W. Baish, T. P. Padera, L. L. Munn and R. K. Jain, *Nat. Biomed. Eng.*, 2019, **3**, 230-245.

49. H. T. Nia, M. Datta, G. Seano, P. Huang, L. L. Munn and R. K. Jain, *Nat. Protoc.*, 2018, **13**, 1091-1105.

50. P. Papageorgis, C. Polydorou, F. Mpekris, C. Voutouri, E. Agathokleous, C. P. Kapnissi-Christodoulou and T. Stylianopoulos, *Sci. Rep.*, 2017, **7**, 46140.

51. J. T. Chen, Z. Y. Ding, S. Li, S. Liu, C. Xiao, Z. F. Li, B. X. Zhang, X. P. Chen and X. L. Yang, *Theranostics*, 2021, **11**, 1345-1363.

52. J. T. Chen, S. Li, X. Liu, S. Liu, C. Xiao, Z. J. Zhang, S. Y. Li, Z. F. Li and X. L. Yang, *Nanoscale*, 2021, **13**.

53. R. H. Tao, M. Kobayashi, Y. Z. Yang and E. S. Kleinerman, *Cancers*, 2021, **13**, 2740.

54. W. A. Berg, D. O. Cosgrove, C. J. Dore, F. K. Schafer, W. E. Svensson, R. J. Hooley, R. Ohlinger, E. B. Mendelson, C. Balu-Maestro, M. Locatelli, C. Tourasse, B. C. Cavanaugh, V. Juhan, A. T. Stavros, A. Tardivon, J. Gay, J. P. Henry, C. Cohen-Bacrie and B. E. Investigators, *Radiology*, 2012, **262**, 435-449.

55. M. J. Paszek, N. Zahir, K. R. Johnson, J. N. Lakins, G. I. Rozenberg, A. Gefen, C. A. Reinhart-King, S. S. Margulies, M. Dembo, D. Boettiger, D. A. Hammer and V. M. Weaver, *Cancer Cell*, 2005, **8**, 241-254.

56. M. F. Pang, M. J. Siedlik, S. Han, M. Stallings-Mann, D. C. Radisky and C. M. Nelson, *Cancer Res.*, 2016, **76**, 5277-5287.

57. D. Wirtz, K. Konstantopoulos and P. C. Searson, *Nat. Rev. Cancer*, 2011, **11**, 512-522.

58. A. Pathak and S. Kumar, *Proc. Natl. Acad. Sci. U. S. A.*, 2012, **109**, 10334-10339.

59. D. Collen, D. C. Stump and H. K. Gold, *Annu. Rev. Med.*, 1988, **39**, 405-423.

60. S. A. Rouf, M. Moo-Young and Y. Chisti, *Biotechnol. Adv.*, 1996, **14**, 239-266.

61. H. Zhang, Y. Yu, L. Zhou, J. Ma, K. Tang, P. Xu, T. Ji, X. Liang, J. Lv, W. Dong, T. Zhang, D. Chen, J. Xie, Y. Liu and B. Huang, *Cancer Immunol. Res.*, 2018, **6**, 1046-1056.

62. M. Altinbas, H. S. Coskun, O. Er, M. Ozkan, B. Eser, A. Unal, M. Cetin and S. Soyuer, *J. Thromb. Haemost.*, 2004, **2**, 1266-1271.

63. R. Di Liello, L. Arenare, F. Raspagliesi, G. Scambia, C. Pisano, N. Colombo, S. Frezzini, G. Tognon, G. Artioli, A. Gadducci, R. Lauria, A. Ferrero, S. Cinieri, A. De Censi, E. Breda, P. Scollo, U. De Giorgi, A. A. Lissoni, D. Katsaros, D. Lorusso, V. Salutari, S. C. Cecere, M. Lapresa, M. Nardin, G. Bogani, M. Distefano, S. Greggi, P. Gargiulo, C. Schettino, C. Gallo, G. Daniele, D. Califano, F. Perrone, S. Pignata and M. C. Piccirillo, *Int. J. Gynecol. Cancer*, 2021, **31**, 1348-1355.

64. S. Rodrigues, L. Cardoso, A. M. R. da Costa and A. Grenha, *Materials*, 2015, **8**, 5647-5670.

65. F. Danhier, E. Ansorena, J. M. Silva, R. Coco, A. Le Breton and V. Preat, *J. Control. Release*, 2012, **161**, 505-522.

66. J. K. Guan, Y. X. Wu, H. M. Wang, H. W. Zeng, Z. F. Li and X. L. Yang, *Nanoscale*, 2021, **13**, 19399-19411.

67. Q. Y. Hu, C. G. Qian, W. J. Sun, J. Q. Wang, Z. W. Chen, H. N. Bomba, H. L. Xin, Q. D. Shen and Z. Gu, *Adv. Mater.*, 2016, **28**, 9573-9580.

68. H. T. Nia, L. L. Munn and R. K. Jain, *Science*, 2020, **370**, eaaz0868.

69. V. P. Chauhan, Y. Boucher, C. R. Ferrone, S. Roberge, J. D. Martin, T. Stylianopoulos, N. Bardeesy, R. A. DePinho, T. P. Padera, L. L. Munn and R. K. Jain, *Cancer Cell*, 2014, **26**, 14-15.

70. F. Mpekris, M. Panagi, C. Voutouri, J. D. Martin, R. Samuel, S. Takahashi, N. Gotohda, T. Suzuki, P. Papageorgis, P. Demetriou, C. Pierides, L. Koumas, P. Costeas, M. Kojima, G. Ishii, A. Constantinidou, K. Kataoka, H. Cabral and T. Stylianopoulos, *Adv. Sci.*, 2021, **8**, 2001917.

71. M. Plodinec, M. Loparic, C. A. Monnier, E. C. Obermann, R. Zanetti-Dallenbach, P. Oertle, J. T. Hyotyla, U. Aebi, M. Bentires-Alj, R. Y. H. Lim and C. A. Schoenenberger, *Nat. Nanotechnol.*, 2012, **7**, 757-765.

72. J. Liu, Y. H. Tan, H. F. Zhang, Y. Zhang, P. W. Xu, J. W. Chen, Y. C. Poh, K. Tang, N. Wang and B. Huang, *Nat. Mater.*, 2012, **11**, 734-741.

73. J. K. Mouw, Y. Yui, L. Damiano, R. O. Bainer, J. N. Lakins, I. Acerbi, G. Q. Ou, A. C. Wijekoon, K. R. Levental, P. M. Gilbert, E. S. Hwang, Y. Y. Chen and V. M. Weaver, *Nat. Med.*, 2014, **20**, 360-367.

74. J. J. Northey, L. Przybyla and V. M. Weaver, *Cancer Discov.*, 2017, **7**, 1224-1237.

75. K. R. Levental, H. Yu, L. Kass, J. N. Lakins, M. Egeblad, J. T. Erler, S. F. Fong, K. Csiszar, A. Giaccia, W. Weninger, M. Yamauchi, D. L. Gasser and V. M. Weaver, *Cell*, 2009, **139**, 891-906.

76. S. C. Wei, L. Fattet, J. H. Tsai, Y. Guo, V. H. Pai, H. E. Majeski, A. C. Chen, R.

L. Sah, S. S. Taylor, A. J. Engler and J. Yang, *Nat. Cell Biol.*, 2015, **17**, 678-688.

77. J. C. Tung, J. M. Barnes, S. R. Desai, C. Sistrunk, M. W. Conklin, P. Schedin, K. W. Eliceiri, P. J. Keely, V. L. Seewaldt and V. M. Weaver, *Free Radic. Biol. Med.*, 2015, **79**, 269-280.

78. F. Bordeleau, B. N. Mason, E. M. Lollis, M. Mazzola, M. R. Zanotelli, S. Somasegar, J. P. Califano, C. Montague, D. J. LaValley, J. Huynh, N. Mencia-Trinchant, Y. L. Negron Abril, D. C. Hassane, L. J. Bonassar, J. T. Butcher, R. S. Weiss and C. A. Reinhart-King, *Proc. Natl. Acad. Sci. U. S. A.*, 2017, **114**, 492-497.

79. T. Stylianopoulos, L. L. Munn and R. K. Jain, *Trends Cancer*, 2018, **4**, 292-319.